# CRK2 enhances salt tolerance in Arabidopsis thaliana by regulating endocytosis and callose deposition in connection þÿ w i t h P L D ± 1

Hunter, Kerri Alyssa

2019-08

Hunter , K A , Kimura , S , Rokka , A , Tran , H C , Toyota , M , Kukkonen , J P & Wrzaczek , M A 2019 , ' CRK2 enhances salt tolerance in Arabidopsis thaliana by regulating endocytosis þÿ a n d c a l l o s e d e p o s i t i o n i n c o n n e c t i o n w i t h P L D ± 1 ' , P l a n t P h y s i o l o g y , þÿ 2 0 0 4 2 0 2 1 . h t t p s : / / d o i . o r g / 1 0 . 1 1 0 1 / 4 8 7 0 0 9 , h t t p s : / / d o i . o r g / 1 0 . 1 1 0 4 / p

http://hdl.handle.net/10138/325045
https://doi.org/10.1101/487009

unspecified
publishedVersion

# CRK2 Enhances Salt Tolerance by Regulating Callose Deposition in Connection with PLDα1[1][OPEN]

**Kerri Hunter,[a] Sachie Kimura,[a] Anne Rokka,[b] Huy Cuong Tran,[a,2] Masatsugu Toyota,[c,d] Jyrki P. Kukkonen,[e,f] and Michael Wrzaczek[a,3,4]**

[a]Viikki Plant Science Centre, Organismal and Evolutionary Biology Research Programme, Faculty of Biological and Environmental Sciences, University of Helsinki, Helsinki, Finland
[b]Turku Centre for Biotechnology, University of Turku and Åbo Akademi University, Turku, Finland
[c]Department of Biochemistry and Molecular Biology, Saitama University, Saitama, Japan
[d]Department of Botany, University of Wisconsin-Madison, Madison, Wisconsin
[e]Biochemistry and Cell Biology, Department of Veterinary Biosciences, Faculty of Veterinary Medicine, University of Helsinki, Helsinki, Finland
[f]Department of Physiology, Faculty of Medicine, University of Helsinki, Helsinki, Finland

**ORCID IDs: 0000-0002-2285-6999 (K.H.); 0000-0001-5736-2123 (S.K.); 0000-0003-1482-9154 (A.R.); 0000-0002-7670-2215 (H.C.T.); 0000-0002-9544-0978 (M.T.); 0000-0002-6989-1564 (J.P.K.); 0000-0002-5946-9060 (M.W.).**

High salinity is an increasingly prevalent source of stress to which plants must adapt. The receptor-like protein kinases, including members of the Cys-rich receptor-like kinase (CRK) subfamily, are a highly expanded family of transmembrane proteins in plants that are largely responsible for communication between cells and the extracellular environment. Various CRKs have been implicated in biotic and abiotic stress responses; however, their functions on a cellular level remain largely uncharacterized. Here we have shown that CRK2 enhances salt tolerance at the germination stage in Arabidopsis (*Arabidopsis thaliana*) and also modulates root length. We established that functional CRK2 is required for salt-induced callose deposition. In doing so, we revealed a role for callose deposition in response to increased salinity and demonstrated its importance for salt tolerance during germination. Using fluorescently tagged proteins, we observed specific changes in the subcellular localization of CRK2 in response to various stress treatments. Many of CRK2's cellular functions were dependent on phospholipase D activity, as were the subcellular localization changes. Thus, we propose that CRK2 acts downstream of phospholipase D during salt stress, promoting callose deposition and regulating plasmodesmal permeability, and that CRK2 adopts specific stress-dependent subcellular localization patterns that allow it to carry out its functions.

[1]This work was supported by the Academy of Finland (grant nos. 275632, 283139, and 312498 to M.W.), the University of Helsinki (three-year fund allocation to M.W.), and KAKENHI (grant nos. 17H05007, 18H04775, and 18H05491 to M.T.). K.H., S.K., and M.W. are members of the Centre of Excellence in the Molecular Biology of Primary Producers (2014–2019) funded by the Academy of Finland (grant nos. 271832 and 307335).

[2]Present address: Department of Biology, Lund University, Sweden

[3]Author for contact: michael.wrzaczek@helsinki.fi.

[4]Senior author.

The author responsible for distribution of materials integral to the findings presented in this article in accordance with the policy described in the Instructions for Authors (www.plantphysiol.org) is: Michael Wrzaczek (michael.wrzaczek@helsinki.fi).

K.H. designed experiments, performed experiments, analyzed data, and wrote the manuscript. S.K., A.R., C.T., and M.T. performed experiments. J.P.K. and M.W. designed experiments. All authors contributed to and edited the final manuscript.

[OPEN]Articles can be viewed without a subscription.

www.plantphysiol.org/cgi/doi/10.1104/pp.19.00560

High soil salinity is becoming increasingly problematic in agriculture, with recent estimates assigning at least 20% of the total cultivatable land as affected (FAO and ITPS, 2015). In order to develop crops that can tolerate such conditions, it is first necessary to understand the mechanisms of salt stress responses and tolerance, much of which remains insufficiently characterized at the cellular and biochemical level. A high-salinity environment exerts an osmotic stress on plants and interferes with soil structure, nutrient and water acquisition, ionic balances, and solute concentrations within cells. This can lead to decreased plant growth, health, yield, and overall agricultural productivity (Shrivastava and Kumar, 2015; Machado and Serralheiro, 2017). Cellular responses to salt stress need to incorporate mechanisms to deal with the physical features of salt stress, such as membrane integrity and osmotic pressure, and the biochemical aspects, such as transport and balance of water, nutrients, solutes, and ions, while maintaining overall plant health and development. The multifaceted response of plant cells to high salinity

 

is currently known to include activation of NADPH oxidase respiratory burst homologs and reactive oxygen species (ROS) production (Ma et al., 2012), calcium influx (Knight et al., 1997; Tracy et al., 2008; Choi et al., 2014), activation of phospholipase D (PLD) and phosphatidic acid (PA) production (Li et al., 2009b; Hong et al., 2010), cell wall modifications (Tenhaken, 2015), changes in plasma membrane composition and formation of microdomains (Wu et al., 1998; Elkahoui et al., 2004; López-Pérez et al., 2009; Hao et al., 2014), and increased endocytosis of various receptors and channels (Baral et al., 2015), notably aquaporins to regulate water transport (Li et al., 2011; Luu et al., 2012; Ueda et al., 2016). The integration and regulation of these processes, however, are still not completely understood.

The receptor-like protein kinases (RLKs) are a highly expanded family of transmembrane proteins in plants, and are largely responsible for communication between cells and the extracellular environment. These proteins are widely represented across plant lineages, with Arabidopsis (*Arabidopsis thaliana*) containing >600 different RLKs (Shiu and Bleecker, 2003). The large diversity of RLKs and potential for cross talk and interaction could permit responses to a huge variety of stimuli; accordingly, RLKs are known to regulate growth, development, and stress adaptation, including the response to pathogens and other biotic and abiotic stimuli (Kimura et al., 2017). RLKs are typically localized at the plasma membrane, with the N-terminal signal perception domain residing in the apoplast and the C-terminal kinase domain extending into the cytoplasm. This orientation permits sensing of extracellular ligands or microenvironment changes and subsequent transmission of the signal to the intracellular environment via the kinase activity or other protein interactions.

Cys-rich receptor-like kinases (CRKs) represent a subgroup of RLKs consisting of 44 members in Arabidopsis (Wrzaczek et al., 2010). CRKs are defined by an extracellular domain containing two copies of the domain of unknown function 26 (DUF26) configuration of conserved cysteines C-X8-C-X2-C (Chen, 2001; Vaattovaara et al., 2019). Based on their expression profile (Wrzaczek et al., 2010) and loss-of-function phenotypes (Bourdais et al., 2015), CRKs are promising signaling candidates for both biotic and abiotic stress-responsive pathways. In particular, CRK2, CRK5, CRK8, CRK11, CRK28, CRK29, CRK36, CRK37, and CRK45 have been implicated in the response to salt stress (Tanaka et al., 2012; Zhang et al., 2013; Bourdais et al., 2015). While some CRKs have been linked to ROS signaling (Idänheimo et al., 2014) and cell death (Burdiak et al., 2015; Yadeta et al., 2017), the majority of their functions on a cellular and biochemical level remain largely uncharacterized.

In this study, we sought to characterize the role of the receptor-like kinase CRK2 during salt stress. We show that CRK2 enhances germination and root length under conditions of high salinity. We describe how the protein acts in connection with PHOSPHOLIPASE D ALPHA 1 (PLD$\alpha$1) to regulate callose deposition in response to salt, and we demonstrate that subcellular protein localization plays a major role in regulating CRK2 function. We also demonstrate salt-induced callose deposition and describe its significance for salt tolerance.

## RESULTS

### CRK2 Interacts with Proteins Involved in Salt Responses

CRK2 was previously linked to multiple stress-related processes (Bourdais et al., 2015), but the mechanisms of its involvement on a biochemical and cellular level remained uncharacterized. RLKs typically do not act alone, but rather in protein complexes. Therefore, we performed a proteomics screen to identify proteins participating in CRK2-containing complexes as an initial step for further characterization of protein function. CRK2-yellow fluorescent protein (YFP)was immunoaffinity purified from seedlings and interacting proteins were identified by mass spectrometry. Unspecific interactors were removed by comparison to the YFP-Myc control line to exclude proteins identified as interacting with YFP. The full list of identified proteins is available in Supplemental Table S1. Experiments were performed under standard growth conditions as well as in NaCl and $H_2O_2$ treatments; however, in most cases no striking differences in identified proteins were noted between the different conditions. The majority of top interactors identified were plasma membrane-associated proteins. Cytoplasmic proteins and extracellular proteins were also considered relevant, as CRK2 contains domains which extend into both the apoplast and the cytoplasm. Nuclear- or organelle-localized proteins identified were considered probable contaminants, which likely came into contact with the bait CRK2-YFP during the protein extraction process.

The identified proteins were annotated for gene ontology classifications based on biological process and analyzed by Singular Enrichment Analysis using the AgriGO GO Analysis Toolkit and Database (China Agricultural University; http://bioinfo.cau.edu.cn/agriGO/) to visualize the processes relevant to the CRK2 interactors (Supplemental Fig. S1; Supplemental Table S2). Several transmembrane channels or transport proteins were identified as top interactors, including multiple aquaporins, ABC type transporters, and ATPases (Supplemental Table S1),

supporting a potential role for CRK2 in the mediation of cellular ionic or osmotic balances. Another protein family which was identified multiple times was the jacalin-related lectins (Supplemental Table S1), which have been shown to be involved in tolerance to both abiotic and biotic stresses (Esch and Schaffrath, 2017). It was shown that secreted proteins with a single DUF26 domain from Gingko and maize bind Man in vitro (Miyakawa et al., 2009, 2014; Ma et al., 2018). In contrast, two related proteins containing tandem DUF26 domains, as is found in CRK2, were not able to bind Man, and ligands of proteins with tandem DUF26 domains remain unknown (Vaattovaara et al., 2019). Therefore, it is conceivable that CRK2 and jacalin-related lectins might participate together in a complex that binds extracellular carbohydrates, glycopeptides, or other extracellular molecules.

Several interesting proteins were identified which were previously implicated in salt stress responses, and a list of selected interactors is presented in Table 1. The selected proteins were chosen based on high confidence scores from mass spectrometry identification, frequency of replicates identified, and references in the literature to salt stress involvement. Many of the top interactors have been linked to salt tolerance, including aquaporins (Bhardwaj et al., 2013), ATPases (Janicka-Russak and Kabała, 2015), and PLD$\alpha$1 (Bargmann et al., 2009). PLD$\alpha$1 was identified as a CRK2-interacting protein in all eight replicates, and was consistently one of the top interactors (Table 1; Supplemental Table S1). PLD$\alpha$1 is mainly located in the cytoplasm in the resting state, and translocates to the plasma membrane upon activation (Wang et al., 2000; Zien et al., 2001). The C-terminal cytoplasmic domain of CRK2 could potentially mediate this docking or, alternatively, could respond to PLD$\alpha$1 docking. Three callose synthases were identified, and while callose deposition has not yet been explicitly documented during salt stress, it is a common feature to many other stress responses, such as pathogen infection (Felix et al., 1999; Gómez-Gómez and Boller, 2000; Jacobs et al., 2003), heavy metal toxicity (O'Lexy et al., 2018), and osmotic stress (Xie et al., 2012). While the callose synthases were only identified in one replicate each, their large protein size and multiple transmembrane regions make these proteins inherently difficult to purify, and thus could account for the relatively low abundance in the samples.

### CRK2 Enhances Salt Tolerance

Previous results indicated a role for CRK2 in salt stress responses, since the transfer DNA (T-DNA) insertion mutant *crk2* (Supplemental Fig. S2) exhibited decreased percentage of germination compared to Col-0 on media containing 150 mM NaCl (Bourdais et al., 2015). We confirmed that *crk2* is more salt sensitive, as assessed by percentage of germination (Fig. 1A), and demonstrated that this phenotype can be rescued by complementation with CRK2-YFP expressed under its native promoter (pCRK2::CRK2-YFP_1-22 and 1-17, in the *crk2* background; Fig. 1A). Overexpression of CRK2-YFP under the control of the *Cauliflower mosaic virus* 35S promoter (35S::CRK2-YFP_9-3, in the Col-0 background) significantly increased salt tolerance at the germination stage (Fig. 1A).

CRK2 contains the conserved motifs of a typical kinase domain (Stone and Walker, 1995;

**Table 1.** *Selected proteins identified as interacting with CRK2*

The 35S::CRK2−YFP_9-3 overexpression line was used in all replicates; unspecific interactors were removed by comparison to the 35S::YFP−Myc_9-6 control line. Each replicate indicates a separate immunoprecipitation in which the protein was identified.

| Locus | Protein | Replicates Identified (Max 8) |
|---|---|---|
| AT3G15730 | PLD$\alpha$1 | 8 |
| AT5G62670 | ATPase 11, plasma membrane-type | 8 |
| AT1G01620 | Aquaporin PIP1-3 | 8 |
| AT3G61430 | Aquaporin PIP1-1 | 7 |
| AT2G37170 | Aquaporin PIP2-2 | 7 |
| AT2G37180 | Aquaporin PIP2-3 | 7 |
| AT4G00430 | Probable aquaporin PIP1-4 | 6 |
| AT4G23400 | Probable aquaporin PIP1-5 | 6 |
| AT5G60660 | Probable aquaporin PIP2-4 | 6 |
| AT2G39010 | Probable aquaporin PIP2-6 | 6 |
| AT4G25960 | ABC transporter B family member 2 | 5 |
| AT1G05570 | CALS1 | 1 |
| AT5G13000 | CALS3 | 1 |
| AT4G03550 | CALS12 | 1 |

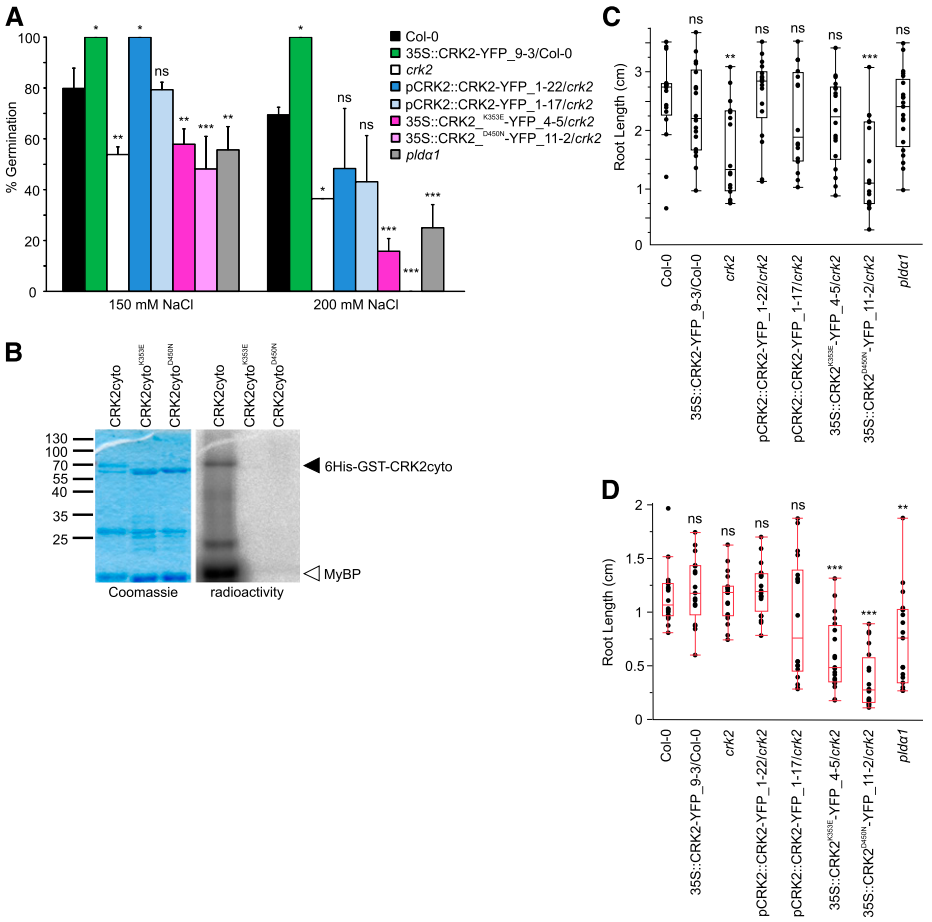


**Figure 1.** CRK2 enhances salt tolerance. A, Overexpression of CRK2 increases salt tolerance at the germination stage; loss of functional CRK2 reduces salt tolerance. Data were normalized to the untreated controls for each line. Comparisons are to Col-0 (one-way ANOVA, post hoc Dunnett); $n = 3$; error bars indicate the SD. B, CRK2 is an active kinase in vitro; kinase-dead protein variants lack kinase activity. C and D, CRK2 is involved in primary root elongation under standard growth conditions (C) and in 150 mM NaCl (D). Comparisons are to Col-0 (one-way ANOVA, post hoc Dunnett); 8-d-old seedlings, transplanted to treatments at 5 d; $n$ = at least 16; box limits represent the 25th and 75th percentiles; the horizontal line represents the median; whiskers extend to the minimal and maximal values. ns, not significant, $^{*}P < 0.05$, $^{**}P < 0.01$, $^{***}P < 0.001$.

Kornev et al., 2006). Using the soluble cytosolic region of CRK2 (CRK2cyto), tagged with glutathione *S*-transferase (GST), we demonstrated that CRK2 is an active kinase in vitro, and is capable of autophosphorylation as well as phosphorylation of the generic kinase substrate myelin basic protein (Fig. 1B). The two mutated variants of CRK2 (CRK2cyto$^{K353E}$ and CRK2cyto$^{D450N}$), which were designed to be kinase dead, did not exhibit kinase activity in vitro (Fig. 1B). These kinase-dead point mutations disable two different motifs typically required for an active kinase: the K353E mutation disrupts the ATP-binding site, whereas the D450N mutation disrupts the catalytic core. Western blot analysis confirmed expression of CRK2-YFP in all transgenic lines (Supplemental Fig. S3A). In order to compare relative protein amounts, the mean intensity of western blot bands was quantified and normalized to Rubisco and Histone H3 as internal controls (Supplemental Fig. S3B).

The germination response to salt is dependent on CRK2 kinase activity; expression of mutated CRK2 variants (kinase-dead; 35S::CRK2$^{K353E}$-YFP and 35S::CRK2$^{D450N}$-YFP, in the *crk2* background) failed to restore the wild-type germination phenotype. In fact, the kinase-dead lines displayed even more severe salt sensitivity than *crk2* (Fig. 1A). The higher salt concentration of 200 mM magnified the differences between the lines, although the overall trend remained largely the same at both concentrations (Fig. 1A). Since PLD$\alpha$1 was identified as a top interactor for CRK2, we also investigated its role in salt stress. The *pld$\alpha$1* mutant line (Supplemental Fig. S2) has been characterized previously as salt sensitive and defective in several cellular processes related to the salt stress response (Bargmann et al., 2009; Yu et al., 2010; Zhang et al., 2012; Hong et al., 2016). Here we show that *pld$\alpha$1* has decreased germination on NaCl-containing media, with a phenotype similar to that of the *crk2* and CRK2 kinase-dead lines (Fig. 1A).

In addition to germination rate, changes in root length and morphology are also associated with salt stress (Julkowska et al., 2014; Kawa et al., 2016; Robin et al., 2016). Assessment of primary root length revealed differences between the CRK2 lines when grown on both untreated and salt-containing media (Fig. 1, C and D). The *crk2* and CRK2$^{D450N}$ lines had significantly shorter roots under standard growth conditions compared to Col-0 (Fig. 1C). Under high-salt conditions, both CRK2 kinase-dead lines had significantly shorter roots compared

to Col-0 (Fig. 1D). The shorter root phenotype was complemented by expression of CRK2-YFP under its native promoter (Fig. 1, C and D). Overexpression of CRK2-YFP under the 35S promoter also complemented the mutant phenotype, but did not further increase root length over that of wild-type or native CRK2 expression (Fig. 1, C and D). The *pldα1* mutant displayed decreased root length compared to Col-0 following NaCl treatment (Fig. 1D). Thus, CRK2 and PLDα1 appear to also be involved in the root length aspect of salt tolerance, and our results suggest that CRK2 kinase activity is important for this function.

NaCl treatment exerts both an osmotic and ionic stress on cells. In order to determine which of these components was more important in relation to CRK2, we tested germination on media containing mannitol or KCl. The results with mannitol were similar to those with NaCl, whereby overexpression of CRK2 leads to higher tolerance (Supplemental Fig. S4). However, *crk2* did not significantly differ from Col-0 when germinated on mannitol (Supplemental Fig. S4). Germination with KCl did not produce any significant differences between the three lines (Supplemental Fig. S4). This suggests that both the osmotic component and $Na^+$ ionic toxicity contribute to the CRK2-mediated NaCl stress response.

### CRK2 Protein Relocalizes in Response to Stress, to Distinct Spots Resembling Plasmodesmata following NaCl Treatment

CRK2 is a transmembrane protein and, like other RLKs, was predicted to localize to the plasma membrane based on the presence of an N-terminal localization signal sequence (Shiu and Bleecker, 2003). Subcellular protein localization was evaluated by live cell imaging using plants expressing a

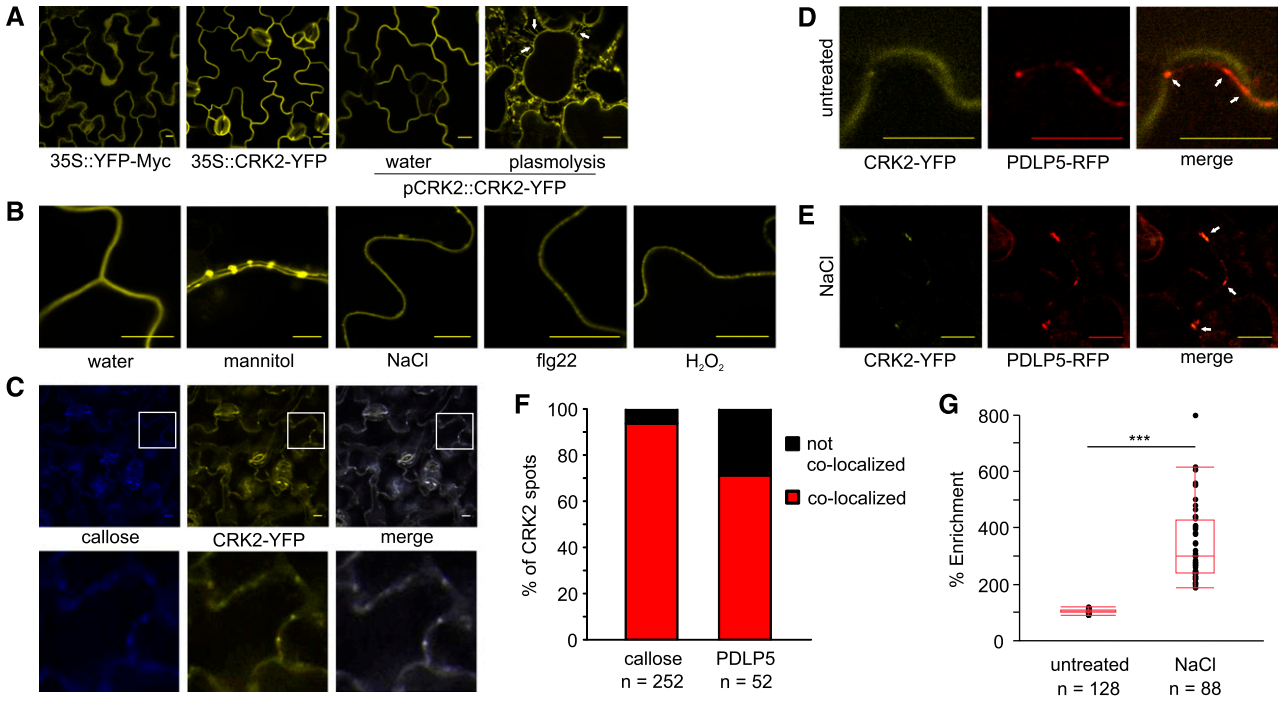


**Figure 2.** CRK2 subcellular protein localization. A, CRK2-YFP localizes uniformly to the plasma membrane under standard growth conditions. Arrows indicate the presence of Hechtian strands following plasmolysis. B, In response to abiotic and biotic stresses, 35S::CRK2-YFP relocalizes to distinct stress-specific patterns along the plasma membrane. Images are of epidermal cells from 7-d-old seedlings; stresses applied were as follows: mannitol, 800 mM for 15 min; NaCl, 150 mM for 30 min; flg22, 10 μM for 30 min; $H_2O_2$, 1 mM for 30 min. C, Colocalization with callose deposits supports NaCl-induced plasmodesmal localization of CRK2-YFP; the white boxes in the upper images indicate the zoomed areas in the lower images. D, CRK2-YFP does not colocalize (arrows) with plasmodesmal marker PDLP5-RFP under standard growth conditions. E, CRK2-YFP partially colocalizes (arrows) with PDLP5-RFP following NaCl treatment. F, Quantification of CRK2-YFP colocalization with callose deposits and PDLP5-RFP following NaCl treatment. Scale bars = 10 μm. G, Quantification of NaCl-induced relocalization of CRK2-YFP by percent enrichment at relocalization domains; box limits represent the 25th and 75th percentiles; the horizontal line represents the median; whiskers extend to the minimal and maximal values; $***P < 0.001$ (one-way ANOVA, pooled *t* test).

35S::CRK2-YFP fusion protein. Under control conditions, CRK2 localized to the cell periphery in epidermal cells (Fig. 2A), in contrast to YFP alone, which localized to the cell periphery, cytoplasm, and nucleus (Fig. 2A). Plasmolysis of cells showed the presence of Hechtian strands (Fig. 2A, arrows), strongly supporting plasma membrane localization of CRK2-YFP. The CRK2 kinase-dead variants displayed a subcellular localization at the plasma membrane similar to that of the wild-type protein (Supplemental Fig. S5).

Controlling protein localization within specific cellular compartments or domains is one means by which cells can regulate protein function post-translationally and adjust activity in response to a stimulus. Localization to specialized domains along the plasma membrane has been observed for other RLKs, including FLAGELLIN SENSITIVE 2 (FLS2) and BRASSINOSTEROID INSENSITIVE 1 (Bücherl et al., 2017). The subcellular localization of CRK2 changed in response to both abiotic and biotic stimuli. The protein assumed a new localization in spots along the plasma membrane, the size and pattern of which depended on the nature of the stress treatment (Fig. 2B). CRK2 expressed under its native promoter showed the same patterns as under the 35S promoter (compare Fig. 2B and Supplemental Fig. S6); therefore, the overexpression line was used for all further analysis of localization. Following treatment with mannitol or NaCl, CRK2 adopted a pattern of concentrated spots along the plasma membrane reminiscent of plasmodesmal localization (Fig. 2B; Thomas et al., 2008; Lee et al., 2011; Xu et al., 2017; Diao et al., 2018). Much of the

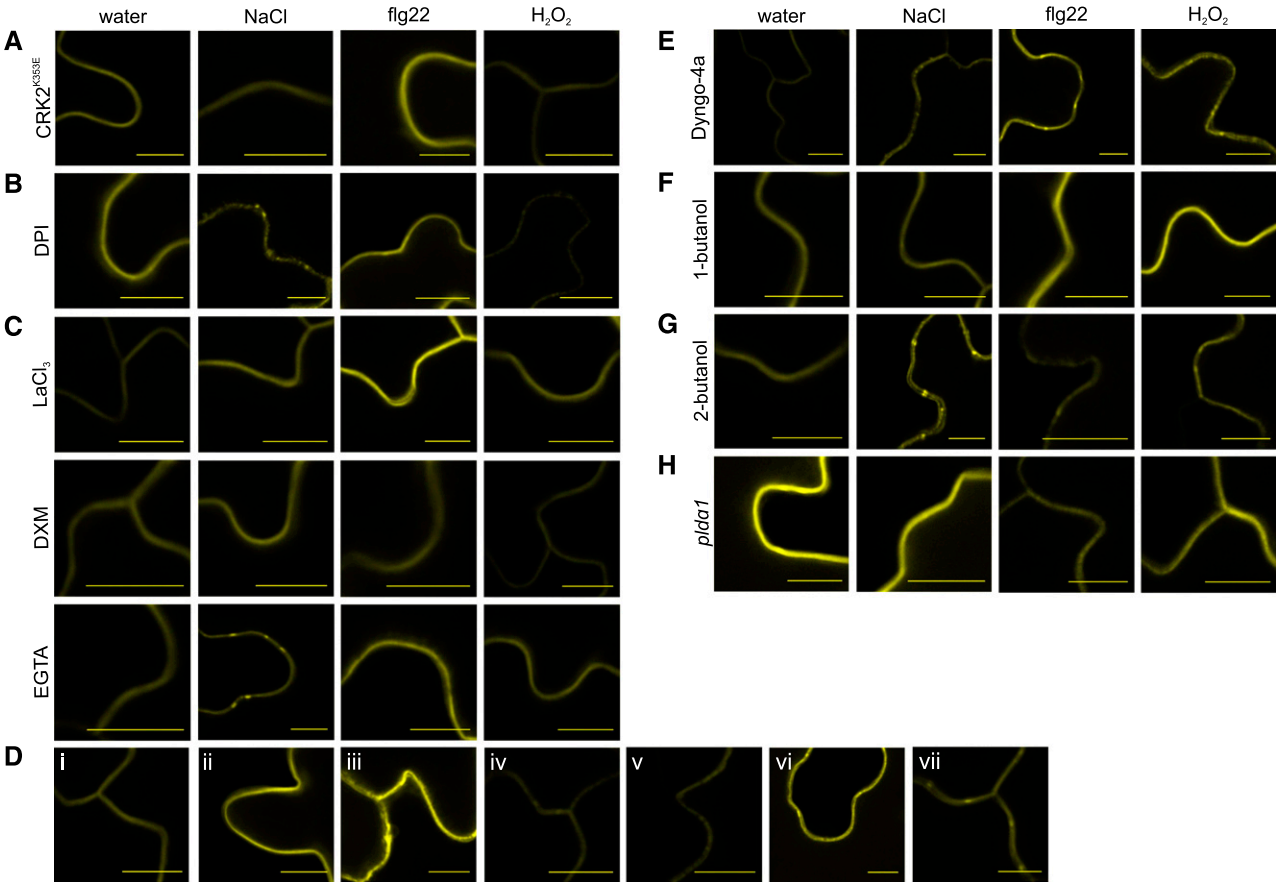


**Figure 3.** Mechanism of CRK2 stress-dependent localization changes. A, Kinase activity is required for both abiotic and biotic stress-induced relocalization. B, NADPH-dependent ROS production is required for the biotic response, but not for the abiotic relocalization. C, Increased cytosolic calcium is required for both abiotic and biotic relocalization. D, Increased cytosolic calcium is sufficient to induce CRK2 relocalization: i, dimethyl sulfoxide (DMSO) control; ii, $CaCl_2$; iii, $CaCl_2$ + ionomycin; iv, CPA; v, DPI + $CaCl_2$ + ionomycin; vi, DPI + CPA; vii, $CRK2^{K353E}$ + $CaCl_2$ + ionomycin. E, Clathrin-mediated internalization is not required for either abiotic or biotic relocalization. F and G, PLD activity is required for both abiotic and biotic relocalization. H, PLDα1 is required for both abiotic and biotic relocalization. 35S overexpression lines were used in all replicates; images are epidermal cells from 7-d-old seedlings; treatment times and conditions are according to Table 2. Scale bars = 10 $\mu$m.

work on relocalization of RLKs has been carried out with microbe-associated molecular pattern treatments. Treatment with flg22, to mimic biotic stress, or $H_2O_2$, to raise the extracellular ROS concentration, produced a localization pattern of smaller, more frequent spots, possibly representing some form of microdomains (Fig. 2B). Localization at plasmodesmata following NaCl treatment was confirmed by colocalization of CRK2-YFP with deposits of callose (Fig. 2C), which is often used as a plasmodesmata marker (Gaudioso-Pedraza and Benitez-Alfonso, 2014; Widana Gamage and Dietzgen, 2017; Xu et al., 2017). Quantification of colocalization revealed that 93.7% of CRK2 spots colocalized with callose deposits following NaCl treatment (Fig. 2F). CRK2-YFP also showed partial colocalization with PLASMODESMATA-LOCATED PROTEIN 5 (PDLP5), which has been previously identified as having a plasmodesmal localization (Lee et al., 2011). CRK2-YFP and PDLP5-RFP did not colocalize under standard growth conditions (Fig. 2D), however, colocalization increased following NaCl treatment (Fig. 2E). The colocalization of CRK2 spots with PDLP5 was 71.2% following NaCl treatment (Fig. 2F). Quantification of CRK2-YFP relocalization was achieved by calculating the percent enrichment at the relocalization domains compared to the rest of the plasma membrane. In untreated samples, there were no discernable differences among different plasma membrane regions, leading to a 1:1 plasmodesmata:nonspecific plasma membrane distribution (Fig. 2G). The enrichment of CRK2-YFP at discernable plasma membrane domains increased significantly following NaCl treatment, with a mean value of 3.4-fold enrichment at plasmodesmata (Fig. 2G).

### CRK2 Relocalization Is Dependent on Intracellular $Ca^{2+}$ and PLD Activity

To study the mechanism of CRK2's stress-induced relocalization patterns, we first investigated the requirement for kinase activity using a kinase-dead variant of CRK2. No changes in localization were observed following NaCl, flg22, or $H_2O_2$ treatment of the kinase-dead line (Fig. 3A), establishing that while CRK2 kinase activity is not required for its delivery to the plasma membrane, it requires an active kinase domain for the relocalization to occur.

ROS and $Ca^{2+}$ are rapidly induced messengers common to numerous stress responses, and they couple to various downstream cellular events. Therefore, we investigated the influence of these components on CRK2 localization using an inhibitor-based approach (Table 2; Supplemental Table S3)

**Table 2.** *Chemicals and experimental conditions*

| Chemical | Function | Concentration | Time | Source |
|---|---|---|---|---|
| 1-butanol | Inhibits phosphatidic acid production by PLD | 0.4% (v/v) | 10 min | Sigma-Aldrich |
| 2-butanol | Negative control for 1-butanol; does not affect PLD | 0.4% (v/v) | 10 min | Alfa Aesar; ThermoFisher |
| $CaCl_2$ | Raises extracellular Ca concentration | 1 mM | 30 min | Merck |
| CPA | Inhibits sarcoendoplasmic reticulum calcium-ATPases, inducing calcium release and secondary store-operated $Ca^{2+}$ influx | 3 $\mu$M | 30 min | Tocris |
| Dextromethorphan | Inhibits $Ca^{2+}$ and $Na^{+}$ channels | 10 $\mu$M | 10 min | RBI; Sigma-Aldrich |
| DMSO | Control for chemicals dissolved in DMSO | 1 $\mu$L | 30 min | Sigma-Aldrich |
| DPI | Inhibits flavoproteins (including respiratory burst homolog s) | 10 $\mu$M | 1 h | Sigma-Aldrich |
| Dyngo-4a | Inhibits dynamin and clathrin-mediated endocytosis | 30 $\mu$M | 10 min | Abcam |
| EGTA | Chelates extracellular $Ca^{2+}$ | 5 mM | 10 min | Sigma-Aldrich, Darmstadt, Germany |
| flg22 | Mimics biotic stress | 10 $\mu$M | 30 min | GenScript |
| $H_2O_2$ | Extracellular ROS treatment | 1 mM | 30 min | Sigma-Aldrich |
| Ionomycin | Induces $Ca^{2+}$ influx | 10 $\mu$M | 30 min | Merck Millipore |
| KCl | Control for NaCl ionic component | 150 mM | 30 min | Fluka; Honeywell |
| $LaCl_3$ | Inhibits $Ca^{2+}$ channels | 1 mM | 10 min | Fluka; Honeywell |
| Mannitol | Osmotic stress, plasmolysis | 800 mM | 15 min | Alfa Aesar; ThermoFisher |
| NaCl | Salt stress | 150 mM | 30 min | Sigma-Aldrich |

whereby the samples were first pretreated with the inhibitor, then subjected to the stress treatments and assessed for localization changes. Inhibition of extracellular ROS production by respiratory burst homologs was achieved with diphenyleneiodonium chloride (DPI), which inhibits flavoenzymes. Under these conditions CRK2-YFP was still able to relocalize upon NaCl treatment, but not upon flg22 treatment (Fig. 3B). This reveals a distinction between the abiotic and biotic stress responses not only in the pattern of localization, but also in the mechanism. Treatment with $H_2O_2$ following DPI pretreatment could still induce the spotted localization response (Fig. 3B). Reduction of calcium signaling, by blocking $Ca^{2+}$ channels with $LaCl_3$ or dextromethorphan, abolished the relocalization response of CRK2-YFP upon both biotic and abiotic stress (Fig. 3C). Chelating extracellular $Ca^{2+}$ with EGTA had a similar effect, but some relocalization was still observed upon NaCl treatment. One explanation is that the $Ca^{2+}$ channel blockers are more efficient than EGTA at preventing $Ca^{2+}$ influx. Alternatively, this could indicate that intracellular $Ca^{2+}$ release also plays a role in addition to $Ca^{2+}$ influx from the extracellular environment (Fig. 3C). Treatment with $H_2O_2$ could no longer induce the response after inhibition of $Ca^{2+}$ channels or chelation of extracellular $Ca^{2+}$, suggesting a presiding need for calcium over ROS for the localization of CRK2-YFP (Fig. 3C). The requirement for a cytosolic $Ca^{2+}$ increase was further supported by the observation that extracellular 1 mM $CaCl_2$ alone was not enough to trigger the relocalization. (Fig. 3D, ii). Cytosolic $Ca^{2+}$ elevation from the apoplast side was achieved by adding $CaCl_2$ + ionomycin and that from the intracellular stores by adding cyclopiazonic acid (CPA); in both cases, relocalization was triggered (Fig. 3D, iii and iv, respectively). Furthermore, $Ca^{2+}$ elevation was stimulated while under the influence of DPI, to block NADPH oxidase-dependent ROS production, and again elevated cytosolic $Ca^{2+}$ was enough to cause relocalization (Fig. 3D, v and vi, respectively). $Ca^{2+}$ elevation also restored the relocalization response in the kinase-dead line (Fig. 3D, vii). These results suggest that elevated intracellular $Ca^{2+}$ is necessary and sufficient to induce the relocalization of CRK2, and likely serves as the primary signal for stress-induced CRK2 localization.

Next, we investigated whether endocytosis was required for CRK2 relocalization, as many RLKs internalize as part of their regulation or signaling functions (Geldner and Robatzek, 2008). Dyngo-4a acts as a dynamin inhibitor to inhibit clathrin-mediated endocytosis (McCluskey et al., 2013). We first tested its effectiveness using the FLS2 receptor, for which internalization upon binding its ligand flg22 is well characterized (Robatzek et al., 2006). Dyngo-4a successfully prevented FLS2-GFP internalization following flg22 treatment and thus functions well in plant cells (Supplemental Fig. S7). Dyngo-4a treatment did not inhibit CRK2-YFP relocalization in response to NaCl, flg22, or $H_2O_2$, suggesting that clathrin-mediated endocytosis is not required for this process (Fig. 3E).

Finally, we examined the involvement of PLD, as these enzymes are capable of altering membrane composition and therefore potentially affect the localization of plasma membrane proteins. We tested the requirement of PLD activity using 1-butanol as an inhibitor of PLD-based PA production. Primary alcohols such as 1-butanol inhibit PLD signaling by acting as a substrate 100-fold preferred over water for utilization in PLD hydrolysis, forcing the reaction in favor of producing phosphatidylbutanol instead of PA (Morris et al., 1997; Gardiner et al., 2003). Pretreatment with 1-butanol effectively blocked CRK2-YFP relocalization in response to NaCl, flg22, and $H_2O_2$, establishing the requirement of PLD-based PA production for CRK2's localization response during both abiotic and biotic stress (Fig. 3F). Because secondary alcohols, such as 2-butanol, do not affect PLD activity, 2-butanol was used as a negative control. As expected, CRK2-YFP relocalization in response to NaCl, flg22, and $H_2O_2$ was not affected by pretreatment with 2-butanol (Fig. 3G). CRK2-YFP transiently expressed in Col-0 seedlings exhibited relocalization responses comparable to those observed in the stable expression line (Supplemental Fig. S8), demonstrating that the transient expression system does not hinder CRK2 relocalization. CRK2-YFP transiently expressed in the *pld$\alpha$1* mutant background was not able to relocalize following NaCl, flg22, or $H_2O_2$ treatments (Fig. 3H). Thus, PLD$\alpha$1 is likely the major PLD isoform facilitating the CRK2 relocalization response to stress treatments.

### CRK2 Is Required for Salt-Induced Callose Deposition

The plasmodesmal localization of CRK2 following salt treatment and the identification of callose synthases as interacting partners prompted the investigation of CRK2's effect on callose deposition. Callose deposition is commonly studied in the context of a stress response, and changes in callose profiles have been observed following bacterial and fungal infection, as well as osmotic stress (Felix et al., 1999; Gómez-Gómez and Boller, 2000; Jacobs et al., 2003; Xie et al., 2012). However, callose deposition in response to acute salt stress has not yet been characterized. We first showed that in wild-type Col-0 plants there was a significant increase in callose deposition in response to NaCl (Fig. 4, A and B). This response was exaggerated in plants

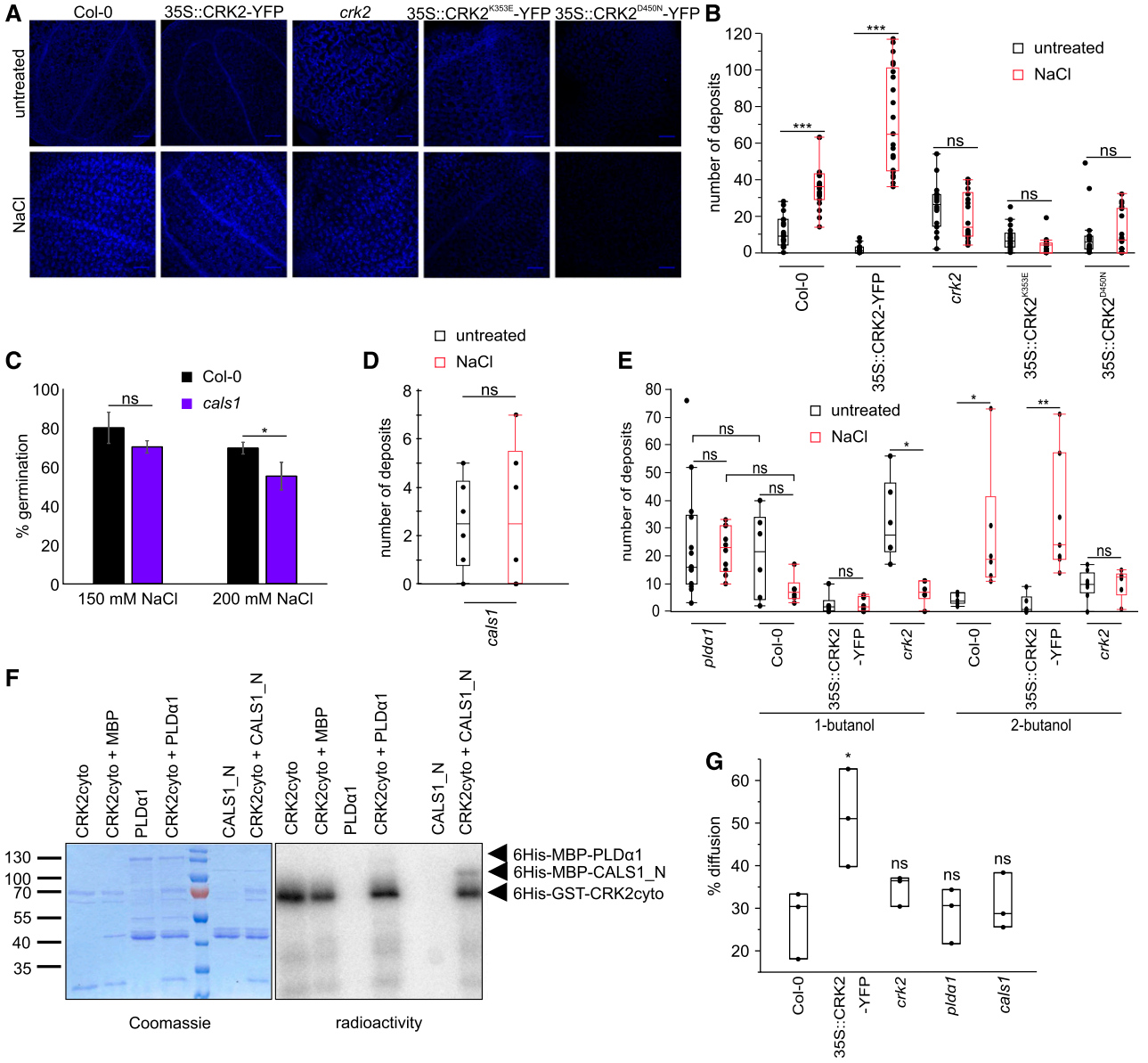


**Figure 4.** CRK2 is required for salt-induced callose deposition. A, Aniline blue staining for callose deposition. Scale bars = 100 $\mu$m. B, Kinase-active CRK2 is required for NaCl-induced callose deposition. The graph shows quantification of callose deposits; comparisons are between untreated and NaCl-treated samples for each line (one-way ANOVA, post hoc Tukey's HSD mean-separation test); $n$ = at least 15. C, Germination of the *cals1* mutant is reduced on salt-containing media. Comparisons are to Col-0 (one-way ANOVA, post hoc Dunnett); error bars indicate the SD; $n = 3$. D, CALS1 is required for NaCl-induced callose deposition. Comparisons are between untreated and NaCl-treated samples (one-way ANOVA, post hoc Tukey's HSD mean-separation test); $n$ = at least 6. E, Impact of PLD on callose deposition in CRK2 lines. Comparisons are between untreated and NaCl-treated samples pretreated with 1-butanol or 2-butanol for each line (one-way ANOVA, post hoc Tukey's HSD mean-separation test); $n \geq 6$. F, CRK2 can phosphorylate the N terminus of CALS1 in vitro but cannot phosphorylate PLDα1. G, Plasmodesmal permeability during standard growth conditions. The observed callose deposition correlates with changes in plasmodesmal permeability. Quantification by percent diffusion of a fluorescent intracellular dye from the adaxial to the abaxial surface; comparisons are to Col-0 (one-way ANOVA, post hoc Dunnett); $n = 3$. Seedlings were 7 d old; the treatment protocol was NaCl, 150 mM for 30 min; box limits represent the 25th and 75th percentiles; the horizontal line represents the median; whiskers extend to the minimal and maxal values; ns, not significant; $^*P < 0.05$, $^{**}P < 0.01$, $^{***}P < 0.001$.

overexpressing CRK2 and lacking in the *crk2* and kinase-dead lines, suggesting that functionally active CRK2 protein is required for a salt-induced callose response (Fig. 4, A and B). We investigated the importance of callose deposition for salt tolerance by assessing germination of the *cals1* mutant (*cals1-5*; Supplemental Fig. S2), which lacks functional CALLOSE SYNTHASE 1 (CALS1). CALS1 is involved in stress response, and regulation of plasmodesmata permeability by CALS1 following pathogen infection and mechanical wounding was demonstrated previously (Cui and Lee, 2016). CALS1 is also one of the callose synthases found to interact with CRK2 and was used here as a representative, since no suitable mutant lines were available for the other identified callose synthases. Germination of *cals1* was reduced on media containing NaCl compared to Col-0 (Fig. 4C). This trend was observed at both concentrations of NaCl, but the difference was only statistically significant at the higher (200 mM) concentration (Fig. 4C). The germination defect was not as severe as with *crk2* (Fig. 1A), likely because of redundancy from the other callose synthases still present. The germination response of additional *cals1-2* and *cals1-3* alleles was similar to that of *cals1-5* and is shown in Supplemental Figure S9. Salt-induced callose deposition is also lacking in *cals1* (Fig. 4D). Together, these results further highlight a role for callose deposition during salt stress, and support CALS1 as a major contributor to salt-induced callose deposition.

The effect of CRK2 on salt-induced callose deposition was associated with active PLD-based PA production. No significant difference was found between the *pldα1* line and 1-butanol-treated Col-0, justifying the interpretation that 1-butanol treatment effectively inhibits PA production by PLD in this assay (Fig. 4E). PLD inhibition did not affect basal callose levels in any of the lines (Fig. 4, B and E), but effectively prevented increases in callose deposition following NaCl treatment in all lines (Fig. 4E). Again, 2-butanol was used as a negative control as it does not inhibit PLD activity. A callose response similar to those in the untreated conditions was observed following 2-butanol pretreatment (Fig. 4E). Therefore, PLD, like CRK2, is required for the salt-induced callose response. Since CRK2 kinase activity was required for the salt-induced callose response, we tested the direct phosphorylation capability of CRK2 in vitro and found that it could phosphorylate CALS1 but not PLDα1 (Fig. 4F). This suggests phosphorylation as a means by which CRK2 might regulate CALS1, and points to CRK2 downstream of PLDα1 and upstream of CALS1 as the mostly likely signaling cascade.

To test whether the observed callose deposition had a biological effect on plasmodesmal permeability, a modified version of the Drop-And-See (DANS) assay was employed (Lee et al., 2011). In this assay a fluorescent intracellular dye is applied to the adaxial surface of the leaf and diffusion to the abaxial surface is assessed, representing the relative

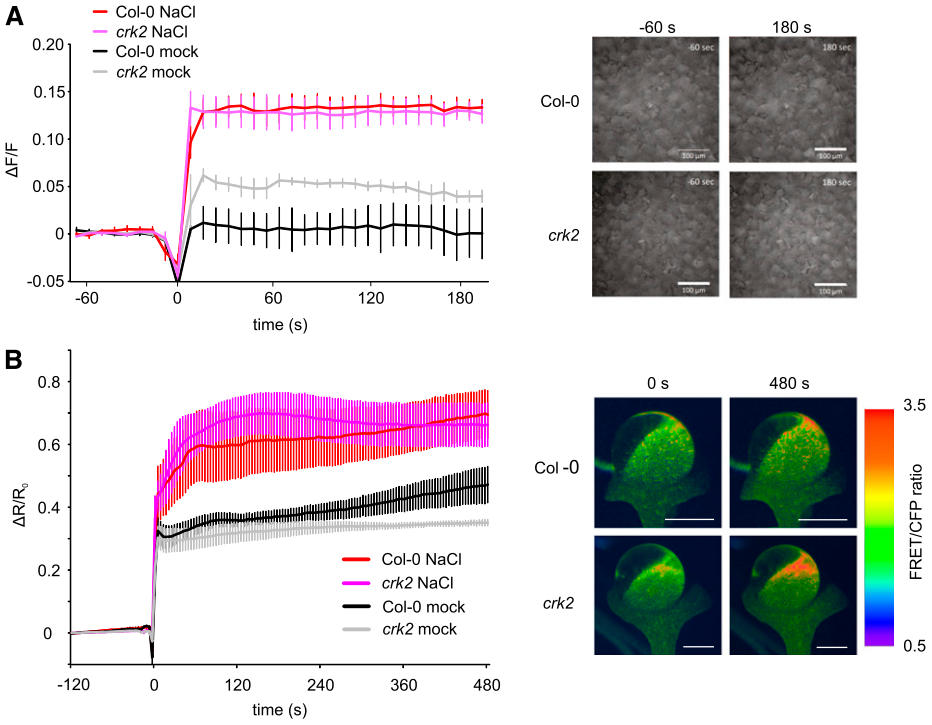


**Figure 5.** CRK2 is not required for the initial salt-induced calcium response. A, Fluo-4-AM calcium imaging of cell-level $Ca^{2+}$ influx in response to 150 mM NaCl in epidermal cells of 7-d-old seedlings; $n = 3$; ~70 cells were measured per replicate. Scale bars = 100 μm. B, YCNano-65 calcium imaging of tissue-level $Ca^{2+}$ influx in response to 150 mM NaCl; 7-d-old seedlings; $n \geq 6$. Scale bars = 1 mm. Additions were made at t = 0. Error bars indicate the SE.

permeability of plasmodesmata. Overexpression of CRK2 resulted in increased plasmodesmal permeability under standard growth conditions (Fig. 4G), in accordance with the decreased basal callose deposition observed in this line (Fig. 4, A and B). The *crk2* line showed an intermediate phenotype where plasmodesmal permeability did not significantly differ from Col-0, perhaps due to genetic redundancy (Fig. 4G). The *pldα1* and *cals1* lines did not significantly differ from Col-0 under standard growth conditions (Fig. 4G), suggesting that their role at plasmodesmata may be relevant primarily during salt stress.

### CRK2 Is Not Required for the Initial Salt-Induced Calcium Response

A common feature between CRK2 relocalization, callose deposition, and PLD activation is the requirement for $Ca^{2+}$. Therefore, we investigated whether CRK2 affected calcium signaling directly using calcium imaging. Fluo-4-AM (Molecular Probes; Thermo Fisher Scientific), a calcium-sensitive fluorescent probe that can be transiently loaded into cells was used to measure the salt-induced calcium response in epidermal cells. The calcium response to NaCl treatment appeared highly similar in both Col-0 and *crk2* (Fig. 5A), suggesting that CRK2 is not likely to play a crucial role in regulation of the initial calcium elevation during salt stress. Interestingly, *crk2* exhibited an increased response to mock treatment when compared to Col-0 (Fig. 5A). This might suggest a higher mechanosensitivity in *crk2*. One drawback of using transient probes is the potential for differential probe loading between samples and genotypes. Therefore, we also used stable transgenic plant lines expressing the Förster resonance energy transfer-based calcium sensor yellow chameleon YCNano-65 (Horikawa et al., 2010). Calcium imaging was performed on the adaxial epidermal tissue layer. Again, no strong differences were observed between YCNano-65/Col-0 and YCNano-65/*crk2* during the initial calcium response to NaCl treatment (Fig. 5B). Together, these results support the hypothesis that CRK2 is not directly affecting the initial calcium signal itself during salt stress, but is acting downstream in a calcium-dependent manner.

## DISCUSSION

Soil affected by high salinity is becoming progressively more widespread, particularly across irrigated agricultural land. This poses an increasing threat to agricultural productivity, as the majority of crop species are not inherently salt tolerant (Yang and Guo, 2018). However, attempts at increasing salt tolerance, through breeding or genetic engineering, must first be preceded by a more thorough understanding of the mechanisms underlying salt tolerance and the molecular pathways involved in salt sensing and cellular responses. As discussed earlier, RLKs are responsible for much of the communication between the extracellular and intracellular environment, and the CRKs specifically have been implicated in various stress responses (Bourdais et al., 2015). Based on phylogenetic analysis, the CRKs can be split into two major groups: basal CRKs and variable CRKs. CRK2 is a member of the basal group of CRKs, which show considerable evolutionary conservation across plant species (Vaattovaara et al., 2019). Large-scale phenotyping of the *crk2* mutant revealed changes in development, biotic stress responses, and abiotic stress responses, including high salinity (Bourdais et al., 2015). Building on this knowledge, the next step is to characterize the specific functions and protein interactions of CRK2 in these processes.

Callose deposition is central to the regulation of plasmodesmal permeability and therefore cell-to-cell communication. This is crucial not only for normal plant development and cellular signaling, but also during adverse conditions where the plant may choose to either close off communication to isolate an affected cell, or open communication to allow distant cells to respond accordingly. Increased callose deposition has been documented for various stresses (Wu et al., 2018), but has not yet been clearly linked to salt stress responses. Here we show that callose deposition is elevated during salt tolerance and the acute response to salt stress, and that NaCl-induced callose deposition is regulated in part by CRK2. Increased CRK2 expression leads to higher levels of callose deposition following salt treatment, and functional, kinase-active CRK2 protein is required for the salt-induced callose response. The CALSs interacting with CRK2 (CALS1, CALS3, and CALS12) all contain at least one predicted phosphorylation site (PhosPhAT 4.0; http://phosphat.uni-hohenheim.de/; Heazlewood et al., 2008; Durek et al., 2010; Zulawski et al., 2013), and CRK2 can phosphorylate CALS1 in vitro. Thus, phosphorylation could be an important means to regulate callose synthase activity and an interesting subject for future research. PLD activity was also required for salt-induced callose deposition; however, it did not affect basal callose levels. This suggests that PLD may not be directly involved in the CRK2-callose synthase interaction, but is more likely exerting its effect upstream in this pathway.

The PLD protein family has been previously associated with salt stress tolerance (Hong et al., 2010). These enzymes cleave phospholipids to

produce PA and a free head group. PLD, along with its product PA, has been linked to a wide range of cellular processes in eukaryotic cells, including endocytosis and vesicle trafficking (Shen et al., 2001; Koch et al., 2004; Lee et al., 2006; Thakur et al., 2016), membrane composition and microdomains (Faraudo and Travesset, 2007), and microtubule and cytoskeletal dynamics (Zhang et al., 2012, 2017). Twelve PLD genes are present in Arabidopsis, of which PLD$\alpha$1 is the major isoform (Pappan et al., 1997a, 1997b, 1998; Qin et al., 1997; Wang and Wang, 2001; Qin and Wang, 2002). Salt stress induces the expression of multiple PLD genes (Katagiri et al., 2001), and the *pld$\alpha$1*, *pld$\alpha$3*, and *pld$\delta$* mutants have been previously characterized as salt sensitive (Hong et al., 2008; Bargmann et al., 2009; Yu et al., 2010). Increased PA concentrations have been documented following various abiotic and biotic stresses, including hyperosmotic stress, salt, drought, freezing, wounding, and pathogens (Testerink and Munnik, 2005). However, in many cases the downstream targets and effectors of PLD/PA signaling are unknown in these responses. PLD$\alpha$1 was consistently found as one of the top interacting proteins with CRK2 and many of the cellular functions of CRK2 are dependent on PLD activity, as are the subcellular localization changes. Arabidopsis lines lacking functional PLD$\alpha$1 or CRK2 have similarly decreased salt tolerance during germination, and several of the CRK2-affected cellular phenotypes have also been linked to PLD$\alpha$1. The inhibitor results and the observation that CRK2 cannot phosphorylate PLD$\alpha$1 support the hypothesis that it is PLD activity, and the accompanying PA production, that is a key factor in the interaction of CRK2 and PLD, rather than a CRK2-directed phosphorylation-based interaction.

PLD activity can influence microtubules and the cytoskeletal structure as part of the response to biotic and abiotic stress. Activation of PLD$\alpha$1 triggers microtubule depolymerization during abscisic acid-induced stomatal closure (Jiang et al., 2014) and stabilizes microtubule organization during salt stress (Zhang et al., 2012). In plant cells, the cytoskeleton extends through plasmodesmata to neighboring cells. Modulation of cytoskeletal components actin and myosin at the neck regions of plasmodesmata may play a role in regulating plasmodesmal permeability, in addition to callose deposition (White and Barton, 2011). It was also shown that different types of plasmodesmata do not all respond the same way to actin and/or myosin inhibitors, and thus the cytoskeleton may also be important for regulating plasmodesmal transport specificity and localizing molecules to plasmodesmata (White and Barton, 2011). PA itself influences membrane properties due to its negative charge, binding capacity for divalent cations (Faraudo and Travesset, 2007), and ability to induce membrane curvature (Kooijman et al., 2003). This curvature is important, for example, during exocytosis and endocytosis, where high degrees of curvature are required for membrane budding and vesicle formation, as well as protein localization (Zhao et al., 2017). PA-rich membrane domains can also directly act as localization signals for PA binding proteins, such as the sphingosine kinase 1 (Delon et al., 2004). Specialized microdomains at plasmodesmata have already been described, and appear essential for targeting of many plasmodesmata-localized proteins (Nicolas et al., 2017; Grison et al., 2019). Thus, PLD, through its action on membrane domains and

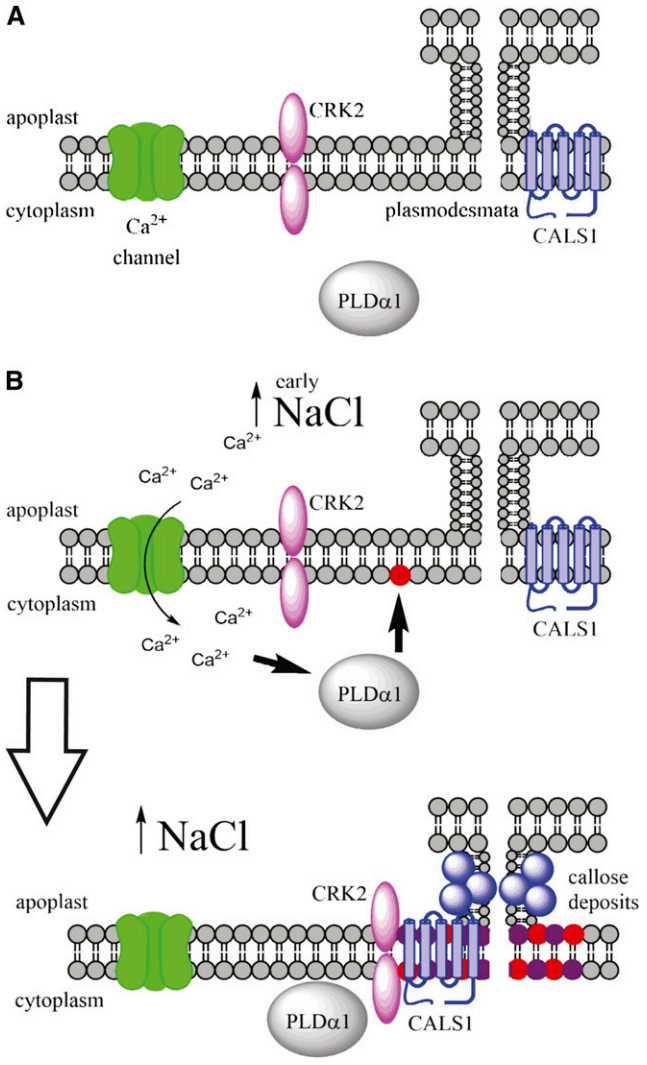


**Figure 6.** Schematic of the proposed pathway for CRK2 regulation of callose deposition at plasmodesmata during salt stress. A, Resting state. B, Early responses to salt stress. Increased extracellular NaCl triggers $Ca^{2+}$ influx. Cytoplasmic $Ca^{2+}$ elevation activates PLD$\alpha$1 leading to PA production and a shift in membrane properties; this serves as a scaffold for changes in CRK2 localization from uniformly along the plasma membrane to specific domains concentrated at plasmodesmata. Once localized at plasmodesmata, CRK2 interacts with CALS1 to promote callose deposition, ultimately leading to enhanced salt tolerance.

cytoskeletal dynamics, could provide a mechanism for the CRK2 localization changes, and for bringing together various components such as CRK2 and CALS1.

In our proposed model, increased extracellular NaCl concentrations would trigger $Ca^{2+}$ influx, as well as ROS production, as one of the earliest initial responses. This $Ca^{2+}$ signal activates PLD$\alpha$1 and causes its translocation from the cytoplasm to the plasma membrane, leading to PA production and a shift in membrane properties (Fig. 6). This would serve as the scaffold for a change in CRK2 localization from uniformly along the plasma membrane to specific domains concentrated at plasmodesmata. Once localized at plasmodesmata, CRK2 interacts with CALS1 to promote callose deposition, ultimately leading to enhanced salt tolerance (Fig. 6). This could explain the observation that NaCl-induced callose deposition—and the variation between the differentially expressed CRK2 lines—is dependent on active PLD, but basal callose deposition is not affected by PLD activity. It also serves to link CRK2 protein function with the dynamic subcellular localization observed.

Here we have shown that CRK2 enhances salt tolerance at the germination stage in Arabidopsis and also increases root length under salt conditions. We demonstrated that CRK2 is involved in the regulation of callose deposition and can interact with CALS1. We found significant differences in callose deposition between wild type, *crk2* mutant, and CRK2 overexpressing lines, and these differences correlate with differences in plasmodesmal permeability, establishing that functional CRK2 is required for salt-induced callose deposition. These findings revealed a role for callose deposition in response to increased salinity, and demonstrated its importance for salt tolerance during germination. Using fluorescently tagged proteins we observed specific changes in CRK2's subcellular localization in response to various stress treatments. These functions and localization are dependent on CRK2 kinase activity, as well as calcium and active PLD-based PA production. Thus, we propose that CRK2 acts downstream of PLD$\alpha$1 during salt stress to promote callose deposition and regulate plasmodesmal permeability, and that it adopts specific stress-dependent subcellular localization patterns in order to carry out its functions.

## MATERIALS AND METHODS

### Growth Conditions

For all experiments, seeds were surface sterilized and plated under sterile conditions on one-half strength Murashige and Skoog media (Sigma-Aldrich) supplemented with 0.8% (w/v) agar, 1% (w/v) Suc, and 0.1% (w/v) MES, pH 5.8. For selection of transgenic lines, 20 $\mu$g/mL Basta (DL-phosphinothricin; Duchefa Biochemie) and 100 $\mu$g/mL ampicillin were added. Plants were grown in a Sanyo growth chamber with a 16-h light, 8-h dark photoperiod. For the DANS assay, seedlings were transferred to soil (2:1 peat:vermiculite) in the greenhouse after seven days. For seed propagation and transgenic line creation, seeds were germinated on soil in the greenhouse and grown with a 12-h light, 12-h dark photoperiod. All seeds were stratified in darkness at 4°C for at least 2 d.

### Plant Lines and Constructs

Arabidopsis (*Arabidopsis thaliana*) Col-0 was used as wild type for all experiments. T-DNA insertion lines for *crk2* (SALK_012659C; At1g70520), *pld$\alpha$1* (SALK_053785; At3g15730), and *cals1-5* (SAIL_1_H10; At1g05570) were obtained from Nottingham Arabidopsis Stock Centre (University of Nottingham). Additional *cals1-2* and *cals1-3* alleles were obtained from Cui and Lee (2016). Constructs for CRK2-YFP and YFP-Myc fusion proteins were created using the MultiSite Gateway technology (Invitrogen; Thermo Fisher Scientific). The coding sequence of CRK2 was amplified by PCR (forward primer, ATGAAGAAAGAACCTGTCC; reverse primer, TCTACCATAAAAGGAACTTTGTGAG) and inserted into pDONRzeo (Invitrogen; Thermo Fisher Scientific), then transferred to the pBm43GW (Invitrogen; Thermo Fisher Scientific) expression vector. The promoter region of CRK2 was amplified by PCR (forward primer, GGTTTTAGATCGTGTTAGATATATCA; reverse primer, TTTGTTTTG TTTGATTGAGAAA) and inserted into pDONR4R1 (Invitrogen; Thermo Fisher Scientific), then transferred to pBm43GW. mVenusYFP, RFP, Myc, PDLP5, and the *Cauliflower mosaic virus* 35S promoter were transferred from existing donor vectors into pBm43GW. To create the kinase-dead protein variants, point mutations were introduced into the coding sequence using mutagenic primers on the donor vectors, and then transferred into pBm43GW. Transgenic lines were created via *Agrobacterium*-mediated floral dipping using *Agrobacterium tumefaciens* GV3101_pSoup. CRK2 and YFP overexpression lines were created in Col-0 background and CRK2 complementation and kinase-dead lines were created in the *crk2* background. Transformed seeds were selected by Basta resistance until T3 homozygous lines were obtained. Transgenic lines are identified as follows: 35S::CRK2-YFP_9-3/Col-0, 35S::YFP-Myc_9-6/Col-0, pCRK2::CRK2-YFP_1-22/*crk2*, pCRK2::CRK2-YFP_1-17/*crk2*, 35S::CRK2$^{K353E}$-YFP_4-5/*crk2*, 35S::CRK2$^{D450N}$-YFP_11-2/*crk2*.

### Genotyping and Semiquantitative RT-PCR

Genomic DNA was extracted from 7-d-old seedlings and used as a template for PCR-based genotyping. The extraction buffer consisted of 100 mM Tris-HCl pH 8.0, 50 mM EDTA, and 500 mM NaCl. For reverse transcription quantitative PCR, RNA was extracted from 7-d-old seedlings, followed by cDNA synthesis, as described previously (Bourdais et al., 2015); this cDNA was used as a template for the semiquantitative RT-PCR reactions. PP2AA3 (At1g13320) was used as a reference gene. Primers used for genotyping and RT-PCR are as follows: CRK2 (GCTAACTATGGTCTTGCGCAG, CAAAGATGAATCGATCAAGGC), PLD$\alpha$1 (CAAGGCTGCAAAGTTTCTCTG, CATCAATGCCCTGCACTT AAT), CALS1 (TTAGACATTCAGGGGTTCGTG, GACGAAAACATT GGTTCTCCA), and PP2AA3 (GAGGATGTCTATGGTTGATG, GCCATT CCCATTATAACTG).

### Transient Expression in *Nicotiana benthamiana*

The pFLS2::FLS2-GFP construct was transformed into GV3101_pSoup *Agrobacterium* and infiltrated into the leaves of 6-week-old *N. benthamiana* plants. The C58C1 *Agrobacterium* strain, containing P19, was coinfiltrated at a 1:1 ratio to enhance and prolong expression. The infiltration medium consisted of 10 mM MES, pH 5.6, 10 mM $MgCl_2$, and 200 $\mu$M acetosyringone. The maximum expression was observed at 2 d postinfiltration, and that was the time point used for all experiments. Leaf discs were cut from infiltrated areas and transferred to 12-well plates for treatments (Table 2).

### Transient Transformation of Arabidopsis Seedlings

The constructs 35S::CRK2−YFP_pBm43GW and 35S::PDLP5-RFP_pBm43GW were transformed into GV3101_pSoup Agrobacteria and then transiently

transformed into Arabidopsis seedlings using the FAST cocultivation method (Li et al., 2009a). Following transformation, the seedlings were kept in darkness for 40 h, moved to light for 24 h, and then analyzed by microscopy as 7-d-old seedlings.

## Immunoprecipitation and Mass Spectrometry

Immunoprecipitation experiments were performed as described previously (Zwiewka et al., 2011; De Rybel et al., 2013), using 0.5 g of 7-d-old seedlings collected under normal conditions, NaCl, or $H_2O_2$ treatments (Table 2). Interacting proteins were isolated from total protein extracts using anti-GFP-coupled magnetic beads (Miltenyi Biotec). Proteins were digested with trypsin to peptides, purified, and sent for identification by mass spectrometry (MS). The MS analyses were performed on a nanoflow HPLC system (Easy-nLC1000, Thermo Fisher Scientific) coupled to the Q Exactive mass spectrometer (Thermo Fisher Scientific). Peptides were first loaded on a trapping column and subsequently separated inline on a 15 cm C18 column (75 $\mu$m × 15 cm, ReproSil-Pur 5 $\mu$m 200 Å C18-AQ). The mobile phase consisted of water with 0.1% (v/v) formic acid (solvent A) or acetonitrile/water (80:20 [v/v]) with 0.1% (v/v) formic acid (solvent B). A 50 min gradient from 6% to 43% B was used to elute peptides. A constant 300 nL/min flow rate was used. MS data were acquired automatically using Thermo Xcalibur 4.0 software (Thermo Fisher Scientific). A data-dependent acquisition method consisted of an Orbitrap MS survey scan of mass range 300–1,800 mass-to-charge ratio, followed by HCD fragmentation for the 10 most intense peptide ions. Data files were searched for protein identification using Proteome Discoverer 2.1 software (Thermo Fisher Scientific) connected to an in-house server running the Mascot 2.5.1 search engine (Matrix Science). The data were searched against the TAIR10 database. The 35S::CRK2-YFP_9-3 overexpression line was used in all replicates. Unspecific interactors were removed by comparison to the 35S::YFP-Myc_9-6 control line to exclude proteins identified as interacting with YFP. Only proteins with more than one peptide were considered as true identifications.

## Germination Assay

Seeds were germinated on either untreated medium or medium treated with 150 mM NaCl or 200 mM NaCl and assessed on day 6. Percent germination was calculated by counting the number of germinated seeds versus total seeds. The untreated samples were set as 100% germination to allow for normalization of data and comparison between lines. Statistical significance was determined by one-way ANOVA with post hoc Dunnett's test using JMP Pro 13 (SAS Institute Inc.). Three replicates were performed for each line and treatment.

## Root Length Assay

Seeds were germinated on regular growth media and transplanted on day 5 to either untreated or 150 mM NaCl medium. Plates were grown in a vertical position and primary root length was measured on day 8. Statistical significance was determined by one-way ANOVA with post hoc Dunnett's test using JMP Pro 13. Replicates are as indicated in the figure legends.

## Western Blot

Following treatments, plant material was immediately frozen in liquid nitrogen and ground to a fine powder. Total proteins were extracted with SDS extraction buffer (50 mM Tris-HCl, pH 7.5, 2% [w/v] SDS, 1% [w/v] protease inhibitor cocktail [Sigma-Aldrich]) and centrifuged at 4°C, 16,000 × *g* for 20 min. Supernatants were loaded in equal protein concentrations and resolved by SDS-PAGE, then transferred to Immobilon-FL polyvinylidene difluoride membranes (Merck Millipore). Western blotting was carried out using mouse anti-GFP 11814460001 (Roche) and rabbit anti-Histone H3 AS10710 (Agrisera) primary antibodies, and goat anti-mouse IRDye800CW (LI-COR) and goat anti-rabbit IRDye800CW (LI-COR) secondary antibodies, and imaged with the Odyssey Infrared Imaging System (LI-COR). Quantification of western blots was carried out in Image J (National Institutes of Health; https://imagej.nih.gov/ij/) by measuring band mean intensity. Col-0 was set as the background level and protein levels were normalized to Rubisco and Histone H3 as internal controls.

## In Vitro Kinase Assay

Constructs for 6His-GST-CRK2cyto (CRK2 cytoplasmic domain), 6His-MBP-PLD$\alpha$1, and 6His-MBP-CALS1_N (CALS1 N terminus) recombinant proteins were generated using In-Fusion technology (Clontech; Takara Bio USA). The fragment of CRK2cyto (wild type, K353E, or D450N) was amplified by PCR (forward primer, AAG TTCTGTTTCAGGGCCCGAAGAGGAAGA GAAGAGGATC; reverse primer, ATGGTCTAGAAAGCTTTATCTACCATA AAAGGAACTTTGTGA) from pDONRzeo-CRK2 plasmid and cloned into pOPINK vector. PLD$\alpha$1 (forward primer, AAGTTCTGTTTCAGGGCCCGA TGGCGCAGCATCTGTTGCACGGG; reverse primer, ATGGTCTAGAAA GCTTTATTAGGTTGTAAGGATTGGAGGCAGG) and CALS1_N (forward primer, AAGTTCTGTTTCAGGGCCCGATGGCTCAAAGAAGGGAAC CTGATC; reverse primer. ATGGTCTAGAAAGCTTTATCTATCAAAACT TCTAAATATATGC) were amplified from cDNA and cloned into pOPINM vector. 6His-GST-CRK2cyto (wild type, K353E, and D450N) were expressed in *Escherichia coli* Lemo21 and purified by Glutathion Sepharose 4B (GE Healthcare). 6His-MBP-PLD$\alpha$1 and 6His-MBP-CALS1_N were expressed in *E. coli* BL21 and purified by Amylose Resin (New England Biolabs). One $\mu$g of kinase protein was incubated in kinase buffer (50 mM HEPES, pH 7.4, 1 mM dithiothreitol, and 10 mM $MgCl_2$) for 30 min at room temperature with [$\gamma$-$^{32}$P]-ATP and substrate protein. Myelin basic protein (Sigma-Aldrich) was used as an artificial substrate. The samples were subsequently separated by SDS-PAGE and exposed to an imaging plate overnight. Radioactivity scans were obtained with Fluor Imager FLA-5100 (Fujifilm).

## Subcellular Protein Localization

Stable homozygous lines expressing mVenusYFP-fusion proteins were used for all live imaging of CRK2. Transient expression of pFLS2::FLS2-GFP in *N. benthamiana* was used for FLS2 internalization controls. Transient transformation of Arabidopsis seedlings was used for CRK2 localization in the *pld$\alpha$1* mutant background and for colocalization with PDLP5. Seven-day-old seedlings were transferred to 12-well plates and treatments were applied as described in Table 2. Samples were mounted in the treatment solution and imaged immediately. Fluorescent images were obtained with a Leica TCS SP5 II HCS confocal microscope using standard YFP settings (CRK2-YFP) of 514 nm excitation and a detection range of 525–590 nm, standard GFP settings (FLS2-GFP) of 488 nm excitation and a detection range of 500–600 nm, or standard RFP settings (PDLP5-RFP) of 561 nm excitation and a detection range of 560–600 nm. Quantification of CRK2 colocalization with callose deposits or PDLP5 was achieved using the following equation: % colocalization = (number of colocalized spots/total number of CRK2 spots). Quantification of CRK2-YFP relocalization was achieved by calculating the percent enrichment at the relocalization domains (with Image J) using the following equation: % enrichment = (fluorescence intensity "spot"/fluorescence intensity general plasma membrane) × 100. Statistical significance was determined by one-way ANOVA with pooled *t* test using JMP Pro 13. Replicates are as indicated in the figure legends.

## Callose Staining

Seven-day-old seedlings were transferred to 12-well plates for treatments (Table 2), then fixed overnight in 1:3 acetic acid:ethanol. Seedlings were washed with 150 mM $K_2HPO_4$ (Sigma-Aldrich) for 30 min and stained with 0.01% (w/v) aniline blue (Sigma-Aldrich) + 150 mM $K_2HPO_4$ for 2 h in darkness. Fluorescent images were obtained with a Leica TCS SP5 II HCS confocal microscope using standard DAPI settings of 405 nm excitation and a detection range of 430–550 nm. The number of callose deposits was counted manually from each image area (780.49 $\mu m^2$). Statistical significance was determined by one-way ANOVA with post hoc Tukey's honestly significant difference (HSD) mean-separation test using JMP Pro 13. Replicates are as indicated in the figure legends. Image intensity was enhanced for visual representation, but all quantifications were made from the original images.

## DANS Assay for Plasmodesmata Permeability

Experiments were performed using a modified version of the DANS assay (Lee et al., 2011). Briefly, rosette leaves were cut from 3-week-old plants and a 1 $\mu$L drop of 5 $\mu$M fluorescein diacetate was applied to the adaxial surface. After 5 min the liquid was removed with filter paper and samples were mounted in water and imaged immediately. Fluorescent images were obtained with a Leica TCS SP5 II HCS confocal microscope using standard GFP settings of 488 nm excitation and a detection range of 500–600 nm. Percent diffusion was calculated by dividing the average total fluorescence from abaxial images by the adaxial images. Statistical significance was determined by one-way ANOVA with post hoc Dunnett's test using JMP Pro 13. Three replicates were performed for each line.

## Calcium Imaging

The fluo-4-AM (Molecular Probes; Thermo Fisher Scientific) synthetic calcium probe was used for cell-level calcium imaging. Cotyledons were removed from 7-d-old seedlings and placed in 96-well plates. Cells were loaded for 1 h at 4°C in darkness, in loading buffer composed of 10 mM MES, 2 mM probenecid, and 5 $\mu$M fluo-4-AM mixed 1:1 with 20% (w/v) pluronic acid. The cotyledons were then washed with experimental buffer (10 mM MES and 2 mM probenecid) and mounted to an open microscope slide chamber, with a 3.0 $\mu$m pore size polycarbonate filter (Polycarbonate 3.0 micron; Osmonics) on top for immobilization (Shariatmadari et al., 2001). Epidermal cells from the adaxial surface were observed. Calcium imaging was performed with a Nikon TE2000 fluorescence microscope. Samples were exposed to 480 nm excitation, and the emitted light was collected through a 505 nm dichroic mirror and a 510–560 nm band-pass filter. Images were acquired every 8 s and treatments were added directly to the chamber during imaging. A final concentration of 150 mM NaCl was used for treatments; mock treatments consisted of experimental buffer. The data were normalized using the following equation: $\Delta F/F_b = (F_t - F_b)/F_b$, where $F_t$ is the fluorescence measured at time point t and $F_b$ is the baseline fluorescence. The baseline was taken as an average of the eight measurements prior to the addition. Approximately 70 cells were measured per run and experiments were repeated three times. Analyses and graphs were made with Microsoft Excel.

Plants expressing the genetically encoded YCNano-65 calcium probe were used for tissue-level calcium imaging. YCNano-65/Col-0 was provided by Prof. Simon Gilroy (University of Wisconsin) and has been previously described (Choi et al., 2014). YCNano-65/*crk2* was generated by crossing YCNano-65/Col-0 with the *crk2* T-DNA mutant. Homozygous F3 lines were selected by Basta resistance (YCNano-65 insertion) and genotyping (T-DNA insertion). Genotyping primers for *crk2* are described by Bourdais et al. (2015))). Seven-day-old seedlings were mounted and 1 $\mu$L of 150 mM NaCl or Murashige and Skoog medium (mock treatment) was applied to the adaxial surface of cotyledons. Calcium imaging was performed with a Nikon SMZ25 microscope using the settings described previously (Lenglet et al., 2017). Cyan fluorescent protein and Förster resonance energy transfer (cpVenus) images were acquired simultaneously every 4 s. Data are presented as the ratio of Förster resonance energy transfer to cyan fluorescent protein signal and were normalized to the initial baseline using the following equation: $\Delta R/Ro = (R_t - Ro)/Ro$, where $R_t$ is the ratio value at time point t and Ro is the initial ratio value. Experiments were repeated at least six times. Analyses and graphs were made with Microsoft Excel.

Schematic figures were made with ChemDraw 16 (PerkinElmer).

## Accession Numbers

The mutant line used in this study, including name, gene, AGI code, and T-DNA insertion line, was as follows: *crk2*, *Crk2*, At1g70520, SALK_012659C; *pldα1*, *Pldα1*, At3g15730, SALK_053785; *cals1-5*, *CalS1*, At1g05570, SAIL_1_H10; *cals1-2*, *CalS1*, At1g05570, SAIL_204_F09; and *cals1-3*, *CalS1*, At1g05570, SALK_152620.

## Supplemental Data

The following supplemental materials are available.

**Supplemental Figure S1.** Gene ontology singular enrichment analysis of identified CRK2 interacting proteins.

**Supplemental Figure S2.** Confirmation of T-DNA mutant lines.

**Supplemental Figure S3.** Protein expression in CRK2 transgenic lines.

**Supplemental Figure S4.** The osmotic component has a greater effect than the ionic component on the CRK2-mediated germination phenotype.

**Supplemental Figure S5.** CRK2-YFP kinase-dead variants have proper subcellular localization.

**Supplemental Figure S6.** CRK2 expressed under its native promoter shows the same localization patterns as the overexpression line.

**Supplemental Figure S7.** Dyngo-4a effectively inhibits FLS2 internalization following flg22 treatment.

**Supplemental Figure S8.** CRK2 expressed transiently shows the same localization patterns as the stable overexpression line.

**Supplemental Figure S9.** Germination response to salt of additional *cals1* alleles.

**Supplemental Table S1.** Full list of proteins identified as interacting with CRK2.

**Supplemental Table S2.** Gene ontology classifications (Biological Process) for identified CRK2 interacting proteins.

**Supplemental Table S3.** Semiquantification of CRK2-YFP localization changes.

## ACKNOWLEDGMENTS

The authors would like to thank Drs. Alexey Shapiguzov (University of Helsinki, Finland) and Julia Krasensky-Wrzaczek (University of Helsinki, Finland) for critical comments on the manuscript. We thank Tuomas Puukko (University of Helsinki, Finland), Nghia Le Tri (University of Helsinki, Finland), and Jiaqi Wang (Saitama University) for technical assistance, Dr. Riccardo Siligato (University of Helsinki, Finland) and Prof. Ari-Pekka Mähönen (University of Helsinki, Finland) for the Gateway Multisite vector system, and Prof. Jung-Youn Lee (University of Delaware) for the *cals1* mutant seeds. PDLP5-RFP seeds were kindly provided by Dr. Fritz Kragler (Max Planck Institute of Molecular Plant Physiology, Germany) and Prof. Marek Mutwil (Nanyang Technological University, Singapore). Microscopy imaging was performed at the Light Microscopy Unit, Institute of Biotechnology, University of Helsinki. Mass spectrometry analyses were performed at the Turku Proteomics Facility, supported by Biocenter Finland.

Received May 10, 2019; accepted May 15, 2019; published May 22, 2019.

## LITERATURE CITED

**Baral A, Irani NG, Fujimoto M, Nakano A, Mayor S, Mathew MK** (2015) Salt-induced remodeling of spatially restricted clathrin-independent endocytic pathways in Arabidopsis root. Plant Cell **27:** 1297–1315

**Bargmann BOR, Laxalt AM, ter Riet B, van Schooten B, Merquiol E, Testerink C, Haring MA, Bartels D, Munnik T** (2009) Multiple PLDs required for high salinity and water deficit tolerance in plants. Plant Cell Physiol **50:** 78–89

**Bhardwaj R, Sharma I, Kanwar M, Sharma R, Handa N, Kaur H, Kapoor D, Poonam**, 2013. Aquaporins: Role under salt stress in plants. *In* P Ahmad, MM Azooz, MNV Prasad, eds, Ecophysiology and Responses of Plants under Salt Stress. Springer, New York, pp. 213–248.

**Bourdais G, Burdiak P, Gauthier A, Nitsch L, Salojärvi J, Rayapuram C, Idänheimo N, Hunter K, Kimura S, Merilo E, et al; CRK Consortium** (2015) Large-scale phenomics identifies primary and fine-tuning roles for CRKs in responses related to oxidative stress. PLoS Genet **11:** e1005373

**Bücherl CA, Jarsch IK, Schudoma C, Segonzac C, Mbengue M, Robatzek S, MacLean D, Ott T, Zipfel C** (2017) Plant immune and growth

receptors share common signalling components but localise to distinct plasma membrane nanodomains. eLife **6:** 6

**Burdiak P, Rusaczonek A, Witoń D, Głów D, Karpiński S** (2015) Cysteine-rich receptor-like kinase CRK5 as a regulator of growth, development, and ultraviolet radiation responses in *Arabidopsis thaliana.* J Exp Bot **66:** 3325–3337

**Chen Z** (2001) A superfamily of proteins with novel cysteine-rich repeats. Plant Physiol **126:** 473–476

**Choi W-G, Toyota M, Kim S-H, Hilleary R, Gilroy S** (2014) Salt stress-induced $Ca^{2+}$ waves are associated with rapid, long-distance root-to-shoot signaling in plants. Proc Natl Acad Sci USA **111:** 6497–6502

**Cui W, Lee J-Y** (2016) *Arabidopsis* callose synthases CalS1/8 regulate plasmodesmal permeability during stress. Nat Plants **2:** 16034

**Delon C, Manifava M, Wood E, Thompson D, Krugmann S, Pyne S, Ktistakis NT** (2004) Sphingosine kinase 1 is an intracellular effector of phosphatidic acid. J Biol Chem **279:** 44763–44774

**De Rybel B, Möller B, Yoshida S, Grabowicz I, Barbier de Reuille P, Boeren S, Smith RS, Borst JW, Weijers D** (2013) A bHLH complex controls embryonic vascular tissue establishment and indeterminate growth in *Arabidopsis.* Dev Cell **24:** 426–437

**Diao M, Ren S, Wang Q, Qian L, Shen J, Liu Y, Huang S** (2018) *Arabidopsis* formin 2 regulates cell-to-cell trafficking by capping and stabilizing actin filaments at plasmodesmata. eLife **7:** 7

**Durek P, Schmidt R, Heazlewood JL, Jones A, MacLean D, Nagel A, Kersten B, Schulze WX** (2010) PhosPhAt: The *Arabidopsis thaliana* phosphorylation site database. An update. Nucleic Acids Res **38:** D828–D834

**Elkahoui S, Smaoui A, Zarrouk M, Ghrir R, Limam F** (2004) Salt-induced lipid changes in *Catharanthus roseus* cultured cell suspensions. Phytochemistry **65:** 1911–1917

**Esch L, Schaffrath U** (2017) An update on jacalin-like lectins and their role in plant defense. Int J Mol Sci **18:** 1592

**FAO and ITPS** (2015) Status of the world's soil resources (SWSR)—Main Report. Food and Agriculture Organization of the United Nations and Intergovernmental Technical Panel on Soils, Rome, Italy

**Faraudo J, Travesset A** (2007) Phosphatidic acid domains in membranes: Effect of divalent counterions. Biophys J **92:** 2806–2818

**Felix G, Duran JD, Volko S, Boller T** (1999) Plants have a sensitive perception system for the most conserved domain of bacterial flagellin. Plant J **18:** 265–276

**Gardiner J, Collings DA, Harper JDI, Marc J** (2003) The effects of the phospholipase D-antagonist 1-butanol on seedling development and microtubule organisation in *Arabidopsis.* Plant Cell Physiol **44:** 687–696

**Gaudioso-Pedraza R, Benitez-Alfonso Y** (2014) A phylogenetic approach to study the origin and evolution of plasmodesmata-localized glycosyl hydrolases family 17. Front Plant Sci **5:** 212

**Geldner N, Robatzek S** (2008) Plant receptors go endosomal: A moving view on signal transduction. Plant Physiol **147:** 1565–1574

**Gómez-Gómez L, Boller T** (2000) FLS2: An LRR receptor-like kinase involved in the perception of the bacterial elicitor flagellin in *Arabidopsis.* Mol Cell **5:** 1003–1011

**Grison MS, Kirk P, Brault M, Wu XN, Schulze WX, Benitez-Alfonso Y, Immel F, Bayer E** (2019) Plasma membrane associated receptor like kinases relocalise to plasmodesmata in response to osmotic stress. Plant Physiol doi:10.1104/pp.19.00473

**Hao H, Fan L, Chen T, Li R, Li X, He Q, Botella MA, Lin J** (2014) Clathrin and membrane microdomains cooperatively regulate RbohD dynamics and activity in *Arabidopsis.* Plant Cell **26:** 1729–1745

**Heazlewood, JL, Durek, P, Hummel, J, Selbig, J, Weckwerth, W, Walther, D, Schulze, WX**2008. PhosPhAt : A database of phosphorylation sites in Arabidopsis thaliana and a plant-specific phosphorylation site predictor. Nucleic Acids Res.**36:** D1015–D1021

**Hong Y, Pan X, Welti R, Wang X** (2008) Phospholipase D$\alpha$3 is involved in the hyperosmotic response in Arabidopsis. Plant Cell **20:** 803–816

**Hong Y, Zhang W, Wang X** (2010) Phospholipase D and phosphatidic acid signalling in plant response to drought and salinity. Plant Cell Environ **33:** 627–635

**Hong Y, Zhao J, Guo L, Kim S-C, Deng X, Wang G, Zhang G, Li M, Wang X** (2016) Plant phospholipases D and C and their diverse functions in stress responses. Prog Lipid Res **62:** 55–74

**Horikawa K, Yamada Y, Matsuda T, Kobayashi K, Hashimoto M, Matsuura T, Miyawaki A, Michikawa T, Mikoshiba K, Nagai T** (2010) Spontaneous network activity visualized by ultrasensitive $Ca^{2+}$ indicators, yellow Cameleon-Nano. Nat Methods **7:** 729–732

**Idänheimo N, Gauthier A, Salojärvi J, Siligato R, Brosché M, Kollist H, Mähönen AP, Kangasjärvi J, Wrzaczek M** (2014) The *Arabidopsis thaliana* cysteine-rich receptor-like kinases CRK6 and CRK7 protect against apoplastic oxidative stress. Biochem Biophys Res Commun **445:** 457–462

**Jacobs AK, Lipka V, Burton RA, Panstruga R, Strizhov N, Schulze-Lefert P, Fincher GB** (2003) An Arabidopsis callose synthase, GSL5, is required for wound and papillary callose formation. Plant Cell **15:** 2503–2513

**Janicka-Russak M, Kabała K** (2015) The role of plasma membrane H+-ATPase in salinity stress of plants. *In* U Lüttge, W Beyschlag, eds, Progress in Botany, **Vol 76**. Springer International Publishing, Cham, Switzerland, pp 77–92

**Jiang Y, Wu K, Lin F, Qu Y, Liu X, Zhang Q** (2014) Phosphatidic acid integrates calcium signaling and microtubule dynamics into regulating ABA-induced stomatal closure in *Arabidopsis.* Planta **239:** 565–575

**Julkowska MM, Hoefsloot HCJ, Mol S, Feron R, de Boer G-J, Haring MA, Testerink C** (2014) Capturing Arabidopsis root architecture dynamics with ROOT-FIT reveals diversity in responses to salinity. Plant Physiol **166:** 1387–1402

**Katagiri T, Takahashi S, Shinozaki K** (2001) Involvement of a novel Arabidopsis phospholipase D, AtPLD$\delta$, in dehydration-inducible accumulation of phosphatidic acid in stress signalling. Plant J **26:** 595–605

**Kawa D, Julkowska MM, Sommerfeld HM, Ter Horst A, Haring MA, Testerink C** (2016) Phosphate-dependent root system architecture responses to salt stress. Plant Physiol **172:** 690–706

**Kimura S, Waszczak C, Hunter K, Wrzaczek M** (2017) Bound by fate: The role of reactive oxygen species in receptor-like kinase signaling. Plant Cell **29:** 638–654

**Knight H, Trewavas AJ, Knight MR** (1997) Calcium signalling in *Arabidopsis thali*ana responding to drought and salinity. Plant J **12:** 1067–1078

**Koch T, Brandenburg L-O, Liang Y, Schulz S, Beyer A, Schröder H, Höllt V** (2004) Phospholipase D2 modulates agonist-induced $\mu$-opioid receptor desensitization and resensitization. J Neurochem **88:** 680–688

**Kooijman EE, Chupin V, de Kruijff B, Burger KNJ** (2003) Modulation of membrane curvature by phosphatidic acid and lysophosphatidic acid. Traffic **4:** 162–174

**Kornev AP, Haste NM, Taylor SS, Eyck LF** (2006) Surface comparison of active and inactive protein kinases identifies a conserved activation mechanism. Proc Natl Acad Sci USA **103:** 17783–17788

**Lee CS, Kim IS, Park JB, Lee MN, Lee HY, Suh P-G, Ryu SH** (2006) The phox homology domain of phospholipase D activates dynamin GTPase activity and accelerates EGFR endocytosis. Nat Cell Biol **8:** 477–484

**Lee J-Y, Wang X, Cui W, Sager R, Modla S, Czymmek K, Zybaliov B, van Wijk K, Zhang C, Lu H, et al** (2011) A plasmodesmata-localized protein mediates crosstalk between cell-to-cell communication and innate immunity in *Arabidopsis.* Plant Cell **23:** 3353–3373

**Lenglet A, Jaślan D, Toyota M, Mueller M, Müller T, Schönknecht G, Marten I, Gilroy S, Hedrich R, Farmer EE** (2017) Control of basal jasmonate signalling and defence through modulation of intracellular cation flux capacity. New Phytol **216:** 1161–1169

**Li J-F, Park E, von Arnim AG, Nebenführ A** (2009a) The FAST technique: A simplified *Agrobacterium*-based transformation method for transient gene expression analysis in seedlings of Arabidopsis and other plant species. Plant Methods **5:** 6

**Li M, Hong Y, Wang X** (2009b) Phospholipase D- and phosphatidic acid-mediated signaling in plants. Biochim Biophys Acta **1791:** 927–935

**Li X, Wang X, Yang Y, Li R, He Q, Fang X, Luu D-T, Maurel C, Lin J** (2011) Single-molecule analysis of PIP2;1 dynamics and partitioning reveals multiple modes of *Arabidopsis* plasma membrane aquaporin regulation. Plant Cell **23:** 3780–3797

**López-Pérez L, Martínez-Ballesta M. del C., Maurel C, Carvajal M** (2009) Changes in plasma membrane lipids, aquaporins and proton pump of

broccoli roots, as an adaptation mechanism to salinity. Phytochemistry **70:** 492–500

**Luu D-T, Martinière A, Sorieul M, Runions J, Maurel C** (2012) Fluorescence recovery after photobleaching reveals high cycling dynamics of plasma membrane aquaporins in Arabidopsis roots under salt stress. Plant J **69:** 894–905

**Ma L, Zhang H, Sun L, Jiao Y, Zhang G, Miao C, Hao F** (2012) NADPH oxidase *AtrbohD* and *AtrbohF* function in ROS-dependent regulation of $Na^+/K^+$ homeostasis in *Arabidopsis* under salt stress. J Exp Bot **63:** 305–317

**Ma L-S, Wang L, Trippel C, Mendoza-Mendoza A, Ullmann S, Moretti M, Carsten A, Kahnt J, Reissmann S, Zechmann B** (2018) The *Ustilago maydis* repetitive effector Rsp3 blocks the antifungal activity of mannose-binding maize proteins. Nat Commun **9:** 1711

**Machado MR, Serralheiro PR** (2017) Soil salinity: Effect on vegetable crop growth. Management practices to prevent and mitigate soil salinization. Horticulturae **3:** 30

**McCluskey A, Daniel JA, Hadzic G, Chau N, Clayton EL, Mariana A, Whiting A, Gorgani NN, Lloyd J, Quan A, et al** (2013) Building a better dynasore: The dyngo compounds potently inhibit dynamin and endocytosis. Traffic **14:** 1272–1289

**Miyakawa T, Miyazono K, Sawano Y, Hatano K, Tanokura M** (2009) Crystal structure of ginkbilobin-2 with homology to the extracellular domain of plant cysteine-rich receptor-like kinases. Proteins **77:** 247–251

**Miyakawa T, Hatano K, Miyauchi Y, Suwa Y, Sawano Y, Tanokura M** (2014) A secreted protein with plant-specific cysteine-rich motif functions as a mannose-binding lectin that exhibits antifungal activity. Plant Physiol **166:** 766–778

**Morris AJ, Frohman MA, Engebrecht J** (1997) Measurement of phospholipase D activity. Anal Biochem **252:** 1–9

**Nicolas WJ, Grison MS, Bayer EM** (2017) Shaping intercellular channels of plasmodesmata: The structure-to-function missing link. J Exp Bot **69:** 91–103

**O'Lexy R, Kasai K, Clark N, Fujiwara T, Sozzani R, Gallagher KL** (2018) Exposure to heavy metal stress triggers changes in plasmodesmatal permeability via deposition and breakdown of callose. J Exp Bot **69:** 3715–3728

**Pappan K, Qin W, Dyer JH, Zheng L, Wang X**1997a. Molecular cloning and functional analysis of polyphosphoinositide-dependent phospholipase D, PLD$\beta$, from Arabidopsis. J. Biol. Chem.**272**, 7055–7061.

**Pappan K, Zheng S, Wang X** (1997b) Identification and characterization of a novel plant phospholipase D that requires polyphosphoinositides and submicromolar calcium for activity in *Arabidopsis*. J Biol Chem **272:** 7048–7054

**Pappan K, Austin-Brown S, Chapman KD, Wang X** (1998) Substrate selectivities and lipid modulation of plant phospholipase D $\alpha$, -$\beta$, and -$\gamma$. Arch Biochem Biophys **353:** 131–140

**Qin C, Wang X** (2002) The Arabidopsis phospholipase D family. Characterization of a calcium-independent and phosphatidylcholine-selective PLD $\zeta$ 1 with distinct regulatory domains. Plant Physiol **128:** 1057–1068

**Qin W, Pappan K, Wang X** (1997) Molecular heterogeneity of phospholipase D (PLD). Cloning of PLD$\gamma$ and regulation of plant PLD$\gamma$, -$\beta$, and -$\alpha$ by polyphosphoinositides and calcium. J Biol Chem **272:** 28267–28273

**Robatzek S, Chinchilla D, Boller T** (2006) Ligand-induced endocytosis of the pattern recognition receptor FLS2 in *Arabidopsis*. Genes Dev **20:** 537–542

**Robin AH, Matthew C, Uddin MJ, Bayazid KN** (2016) Salinity-induced reduction in root surface area and changes in major root and shoot traits at the phytomer level in wheat. J Exp Bot **67:** 3719–3729

**Shariatmadari R, Lund PE, Krijukova E, Sperber GO, Kukkonen JP, Akerman KE** (2001) Reconstitution of neurotransmission by determining communication between differentiated PC12 pheochromocytoma and HEL 92.1.7 erythroleukemia cells. Pflugers Arch **442:** 312–320

**Shen Y, Xu L, Foster DA** (2001) Role for phospholipase D in receptor-mediated endocytosis. Mol Cell Biol **21:** 595–602

**Shiu S-H, Bleecker AB** (2003) Expansion of the receptor-like kinase/Pelle gene family and receptor-like proteins in Arabidopsis. Plant Physiol **132:** 530–543

**Shrivastava P, Kumar R** (2015) Soil salinity: A serious environmental issue and plant growth promoting bacteria as one of the tools for its alleviation. Saudi J Biol Sci **22:** 123–131

**Stone JM, Walker JC** (1995) Plant protein kinase families and signal transduction. Plant Physiol **108:** 451–457

**Tanaka H, Osakabe Y, Katsura S, Mizuno S, Maruyama K, Kusakabe K, Mizoi J, Shinozaki K, Yamaguchi-Shinozaki K** (2012) Abiotic stress-inducible receptor-like kinases negatively control ABA signaling in Arabidopsis. Plant J **70:** 599–613

**Tenhaken R** (2015) Cell wall remodeling under abiotic stress. Front Plant Sci **5:** 771

**Testerink C, Munnik T** (2005) Phosphatidic acid: A multifunctional stress signaling lipid in plants. Trends Plant Sci **10:** 368–375

**Thakur R, Panda A, Coessens E, Raj N, Yadav S, Balakrishnan S, Zhang Q, Georgiev P, Basak B, Pasricha R et al** (2016) Phospholipase D activity couples plasma membrane endocytosis with retromer dependent recycling. eLife **5:** e18515

**Thomas CL, Bayer EM, Ritzenthaler C, Fernandez-Calvino L, Maule AJ** (2008) Specific targeting of a plasmodesmal protein affecting cell-to-cell communication. PLoS Biol **6:** e7

**Tracy FE, Gilliham M, Dodd AN, Webb AAR, Tester M** (2008) NaCl-induced changes in cytosolic free $Ca^{2+}$ in *Arabidopsis thaliana* are heterogeneous and modified by external ionic composition. Plant Cell Environ **31:** 1063–1073

**Ueda M, Tsutsumi N, Fujimoto M** (2016) Salt stress induces internalization of plasma membrane aquaporin into the vacuole in *Arabidopsis thaliana*. Biochem Biophys Res Commun **474:** 742–746

**Vaattovaara A, Brandt B, Rajaraman S, Safronov O, Veidenberg A, Luklová M, Kangasjärvi J, Löytynoja A, Hothorn M, Salojärvi J, et al** (2019) Mechanistic insights into the evolution of DUF26-containing proteins in land plants. Commun Biol **2:** 56

**Wang C, Wang X** (2001) A novel phospholipase D of Arabidopsis that is activated by oleic acid and associated with the plasma membrane. Plant Physiol **127:** 1102–1112

**Wang C, Zien CA, Afitlhile M, Welti R, Hildebrand DF, Wang X** (2000) Involvement of phospholipase D in wound-induced accumulation of jasmonic acid in arabidopsis. Plant Cell **12:** 2237–2246

**White RG, Barton DA** (2011) The cytoskeleton in plasmodesmata: A role in intercellular transport? J Exp Bot **62:** 5249–5266

**Widana Gamage SMK, Dietzgen RG** (2017) Intracellular localization, interactions and functions of Capsicum chlorosis virus proteins. Front Microbiol **8:** 612

**Wrzaczek M, Brosché M, Salojärvi J, Kangasjärvi S, Idänheimo N, Mersmann S, Robatzek S, Karpiński S, Karpińska B, Kangasjärvi J**, 2010. Transcriptional regulation of the CRK/DUF26 group of Receptor-like protein kinases by ozone and plant hormones in Arabidopsis. BMC Plant Biol**10:** 95.

**Wu J, Seliskar DM, Gallagher JL** (1998) Stress tolerance in the marsh plant *Spartina patens*: Impact of NaCl on growth and root plasma membrane lipid composition. Physiol Plant **102:** 307–317

**Wu S-W, Kumar R, Iswanto ABB, Kim J-Y** (2018) Callose balancing at plasmodesmata. J Exp Bot **69:** 5325–5339

**Xie B, Deng Y, Kanaoka MM, Okada K, Hong Z** (2012) Expression of *Arabidopsis* callose synthase 5 results in callose accumulation and cell wall permeability alteration. Plant Sci **183:** 1–8

**Xu B, Cheval C, Laohavisit A, Hocking B, Chiasson D, Olsson TSG, Shirasu K, Faulkner C, Gilliham M** (2017) A calmodulin-like protein regulates plasmodesmal closure during bacterial immune responses. New Phytol **215:** 77–84

**Yadeta KA, Elmore JM, Creer AY, Feng B, Franco JY, Rufian JS, He P, Phinney B, Coaker G** (2017) A cysteine-rich protein kinase associates with a membrane immune complex and the cysteine residues are required for cell death. Plant Physiol **173:** 771–787

**Yang Y, Guo Y** (2018) Elucidating the molecular mechanisms mediating plant salt-stress responses. New Phytol **217:** 523–539

**Yu L, Nie J, Cao C, Jin Y, Yan M, Wang F, Liu J, Xiao Y, Liang Y, Zhang W** (2010) Phosphatidic acid mediates salt stress response by regulation of MPK6 in *Arabidopsis thaliana*. New Phytol **188:** 762–773

**Zhang Q, Lin F, Mao T, Nie J, Yan M, Yuan M, Zhang W** (2012) Phosphatidic acid regulates microtubule organization by interacting with MAP65-1 in response to salt stress in *Arabidopsis*. Plant Cell **24:** 4555–4576

**Zhang Q, Qu Y, Wang Q, Song P, Wang P, Jia Q, Guo J** (2017) Arabidopsis phospholipase D$\alpha$1-derived phosphatidic acid regulates microtubule

organization and cell development under microtubule-interacting drugs treatment. J Plant Res **130:** 193–202

**Zhang X, Yang G, Shi R, Han X, Qi L, Wang R, Xiong L, Li G** (2013) Arabidopsis cysteine-rich receptor-like kinase 45 functions in the responses to abscisic acid and abiotic stresses. Plant Physiol Biochem **67:** 189–198

**Zhao W, Hanson L, Lou H-Y, Akamatsu M, Chowdary PD, Santoro F, Marks JR, Grassart A, Drubin DG, Cui Y, et al** (2017) Nanoscale manipulation of membrane curvature for probing endocytosis in live cells. Nat Nanotechnol **12:** 750–756

**Zien CA, Wang C, Wang X, Welti R** (2001) In vivo substrates and the contribution of the common phospholipase D, PLD$\alpha$, to wound-induced metabolism of lipids in *Arabidopsis*. Biochim Biophys Acta **1530:** 236–248

**Zulawski M, Braginets R, Schulze WX** (2013) PhosPhAt goes kinases—searchable protein kinase target information in the plant phosphorylation site database PhosPhAt. Nucleic Acids Res **41:** D1176–D1184

**Zwiewka M, Feraru E, Möller B, Hwang I, Feraru MI, Kleine-Vehn J, Weijers D, Friml J** (2011) The AP-3 adaptor complex is required for vacuolar function in *Arabidopsis*. Cell Res **21:** 1711–1722